Determining relative block structure rating in the case of non-orthogonal joint sets

Lamine Boumaiza[a]*, Ali Saeidi[a] and Marco Quirion[b]

[a]*Department of Applied Sciences, University of Quebec at Chicoutimi, Chicoutimi (Quebec), G7H 2B1, Canada*

[b]*Department of Dams and Infrastructures, Hydro-Quebec, Montreal (Quebec), H2Z 1A4, Canada*

*Corresponding author: E-mail address: lamine.boumaiza@uqac.ca (L. Boumaiza)

ABSTRACT

The most commonly used method for assessing the hydraulic erodibility of rock is Annandale's method. This method is based on a correlation between the erosive force of flowing water and the capacity of rock resistance. This capacity is evaluated using Kirsten's index, which was initially developed to evaluate the excavatability of earth materials. For rocky material, this index is determined according to certain geomechanical factors related to the intact rock and the rock mass, such as the compressive strength of intact rock, the rock block size, the discontinuity shear strength and the relative block structure. To quantify the relative block structure, Kirsten developed a mathematical expression that accounted for the shape and orientation of the blocks relative to the direction of flow. Kirsten's initial concept for assessing relative block structure considers that the geological formation is mainly fractured by two joint sets forming an orthogonal fractured system. An adjusted concept is proposed to determine the relative block structure when the fractured system is non-orthogonal where the angle between the planes of the two joint set is greater or less than 90°. An analysis of the proposed relative block structure rating shows that considering a non-orthogonal fractured system has a significant effect on Kirsten's index and, as a consequence, on the assessment of the hydraulic erodibility of rock.

Keywords: Fractured rock, Blocky rock, Dip angle, Dip direction, Joint spacing, Relative ground structure, Hydraulic erodibility of rock, Annandale's method, Kirsten's index.

Symbol notation list

A, A', B and B': the coaxial components of force

a: Constant coefficient (a = 5)

b: Constant coefficient (b = 5)

Js: Relative block structure

J_s^p: Required penetration effort

J_s^d: Required dislodging effort

Kb: Rock block size

Kd: Discontinuity shear strength

K_d: Kinematic possibility of dislodgment

K_p: Kinematic possibility of penetration

Ms: Compressive strength of intact rock

N: Kirsten's index

P_r: Required hydraulic stream power

RJS: Ratio of joint spacing (expressed in an equation as $r = S_\Psi/S_\theta$)

RMR: Rock mass rating system

RMSE: Root mean square error

S_θ: Joint spacing of the first joint set

S_Ψ: Joint spacing of the second joint set

θ: Dip angle of the first joint set

Ψ: Dip angle of the second joint set

α: Angle between the planes of two joint sets

λ_θ: Joint frequency of the first joint set

λ_Ψ: Joint frequency of the second joint set

1. Introduction

The assessment of the hydraulic erodibility of earth materials was studied initially for problems associated with the erosion of earth materials under bridges (Keaton, 2013). It has since been adopted for dams given that erosion phenomena can occur on downstream rocks during flood spill periods, as observed at the Tarbela Dam in Pakistan (Lowe et al., 1979) and the Kariba Dam in Zambia (Bollaert et al., 2012). Annandale's method (Annandale 1995, 2006) is the most commonly used method for assessing the hydraulic erodibility of earth materials (Castillo and Carrillo, 2016; Hahn and Drain, 2010; Laugier et al., 2015; Mörén and Sjöberg, 2007; Pells et al., 2015; Rock, 2015). This method is based on a correlation between the erosive force of flowing water, namely the available hydraulic stream power, and the capacity of rock to resist the flow energy. This capacity is evaluated using Kirsten's index (Kirsten, 1988, 1982), which was initially developed to evaluate the excavatability of earth materials but has since been adopted to assess the hydraulic erodibility of earth materials. The interest of using Kirsten's index was first mentioned at a symposium focused on rock mass classification systems (Kirkaldie, 1988), where it was argued that the processes of mechanical excavatability and hydraulic erodibility of earth materials could be considered as similar processes (Moore and Kirsten 1988). Since then, many researchers have analysed the hydraulic erodibility of earth materials by using the excavatability index, where the « direction of excavation » of the original index has been replaced by « direction of flow » (Pitsiou 1990, Doog 1993, Annandale and Kirsten 1994, Moore et al. 1994, Van Schalkwyk et al. 1994, Annandale 1995, Kirsten et al. 2000). Hereinafter, the acronym of « direction of excavation » and the « direction of flow » are considered as synonymous and the term corresponds to the direction of the acting force. For rock material, Kirsten's index (N) is determined according to certain geomechanical factors related to the intact rock and the rock

mass, such as the compressive strength of intact rock (*Ms*), the rock block size (*Kb*), the discontinuity shear strength (*Kd*) and the relative block structure (*Js*). Kirsten's index can be calculated according to Eq. (1):

$$N = Ms \cdot Kb \cdot Kd \cdot Js \quad (1)$$

There are many indices developed for assessing the excavatability of earth materials (MacGregor et al. 1994, Clark 1996, Hadjigeorgiou and Poulin 1998, Basarir and Karpuz 2004). The choice of adopting Kirsten's index is mainly based on its wide range of applications ranging from cohesive and non-cohesive soils to rock (Kirsten et al., 2000). In addition, Van Schalkwyk et al. (1994) tested several rock mass characterization indices and found that they generated similar results, but better accuracy was obtained with Kirsten's index (Pells, 2016). To improve the evaluation of bedrock erosion, Huang et al. (2013) proposed a modification of the erodibility index; they developed a new equation for determining the RQD (Rock Quality Designation) that is included in *Kb* factor. However, the other factors included in Kirsten's index have not had any modifications.

As reported by Pells (2016), Kirsten considers the orientation of a block relative to the direction of flow as an important parameter to be considered in assessing the hydraulic erodibility of rock. Thus, Kirsten has included the « Relative block structure » parameter in his index. This parameter represents the required effort to excavate the rock, and it has been quantified mathematically. Kirsten assumed that geological formations are mainly fractured by two intersecting joint sets, where an angle of 90° is kept between the planes of the two joint sets (orthogonal fractured system). Given that a bulldozer's bucket needs to penetrate the ground surface and then dislodge the blocks of rock during the excavation process, the excavatability of the rock mass can be determined according to the action of ground surface penetration and the

dislodging of rocky blocks. For the latter, Kirsten (1982), developed a concept for blocks oriented against the direction of excavation, and he then generated a mathematical expression for determining the required effort to dislodge the block. It should be noted that Kirsten's (1982) concept is only truly valid for an orthogonal fractured system. However, in practice, Kirsten's index is applied to all cases, including non-orthogonal fractured systems, by assuming a certain lack of precision in terms of the assessment of erodibility. As part of this study, adjustments are introduced to the initial « Relative block structure » concept proposed by Kirsten. The introduced adjustments produce two equations for assessing the required effort to dislodge rocky blocks for a non-orthogonal joint set system. No previous works have proposed adjustments for a non-orthogonal joint set system. One equation is applied when the blocks are oriented in the direction of flow. The second equation is applicable when the blocks are oriented against the direction of flow. This paper first describes the initial « Relative block structure » concept of Kirsten. The second part of this paper then describes the proposed equations, the initial results obtained from these equations and the adjustments made to produce the final *Js* rating for non-orthogonal fractured systems. Given that two joint sets are intersected by both larger and smaller angles than the single 90° angle considered by Kirsten, this paper also presents the effect of a non-orthogonal joint sets system on Kirsten's index and, consequently, on the assessment of the hydraulic erodibility of rock.

2. Relative block structure

Our modifications of Kirsten's index focus on the relative block structure factor. This section describes the initial « Relative block structure » concept of Kirsten, but we include a large review of the underlying concepts that was not included in the initial Kirsten paper. According to Kirsten (1982), the relative orientation of blocks and the spacing of joints affect both the

possibility of penetrating the ground surface and dislodging the individual blocks. Accordingly, Kirsten (1982) determined the effect of orientation and shape of blocks on the excavatability process by considering the kinematic possibility of penetration (K_p) and the kinematic possibility of dislodgment (K_d). The first and second following subsections describe K_p and K_d, respectively, while the third subsection describes the methodology followed by Kirsten to develop the relative block structure rating.

2.1. Kinematic possibility of penetration

K_p is directly related to the inclination of the joints bounding blocks. In practical situations, these blocks can be considered as delineated by two joint sets. The respective dips of these two joint sets relative to the ground surface are labelled as θ and Ψ, while S_θ and S_Ψ represent their respective spacing (Kirsten 1982) (Fig. 1). As the reciprocal of the joint spacing provides the number of joints per unit length, defined as the joint frequency (λ), λ_θ can be given as $1/S_\theta$ and λ_Ψ can be given as $1/S_\Psi$. Accordingly, the dip of the first joint set can be defined as $\tan\theta.\lambda_\theta$ and as $\tan\Psi.\lambda_\Psi$ for the second joint set. As the geological formation is assumed to be fractured by two intersected joint sets, the combined kinematic possibility of penetration is the arithmetic average of the relative dips of joint sets (Eq. 2).

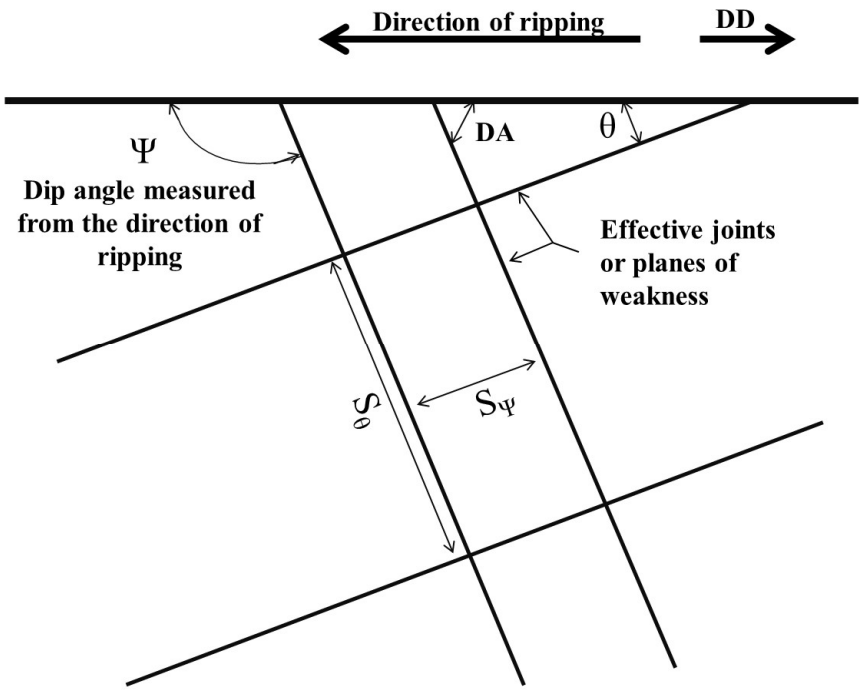

Fig. 1. Model for two joint sets as proposed by Kirsten (1982).

$$K_P = \frac{tan\,\theta\,\lambda_\theta + tan\,\psi\,\lambda_\psi}{\lambda_\theta + \lambda_\psi} \tag{2}$$

By simplifying, K_p can be expressed according to Eq. (3):

$$K_p = \frac{S_\psi\,tan\,\theta + S_\theta\,tan\,\psi}{S_\psi + S_\theta} \tag{3}$$

Given that the ratio of joint spacing (RJS), named r, is equal to S_Ψ/S_θ, Eq. (3) can be expressed as:

$$K_p = \frac{r\,tan\,\theta + tan\,\psi}{a\,(r+1)} \tag{4}$$

The value of a in Eq. (4) is 5 based on empirical assessments of the effects of the direction of ripping on the efficiency of ripping (Kirsten 1982). Furthermore, it is considered by Kirsten (1982) that the sum of K_p and the required penetration effort (J_s^p) is equal to 1 ($K_p + J_s^p = 1$). Therefore, J_s^p can be expressed according to Eq. (5):

$$J_s^p = \left[1 - \frac{r \tan \theta + \tan \psi}{a\,(r+1)} \right] \tag{5}$$

2.2. Kinematic possibility of dislodgement

Once there is penetration into the ground (Fig. 2 portrays a bulldozer, which is moving from right to left), excavatability occurs according to the digging process of angle θ, followed by the riding process of angle Ψ (Fig. 2). The action of block dislodgement can be represented by a horizontal force behind the block while this block is free to move in a perpendicular direction to the ground surface (Kirsten 1982). As a result, K_d as shown in Fig. 3, can be obtained by the vector product of the principal dislodging force and the principal degree of freedom. The vectors of the principal dislodging force and the principal degree of freedom can be decomposed into parallel coaxial components along the sides of the block (Kirsten 1982). The coaxial components are identified as A, B, B' and A' in Fig. 3.

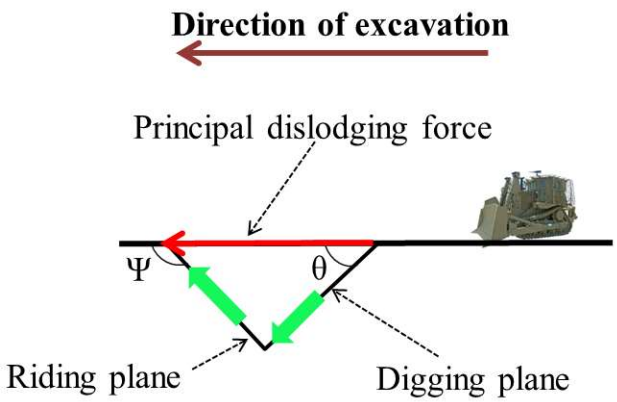

Fig. 2. The principle of the principal dislodging force.

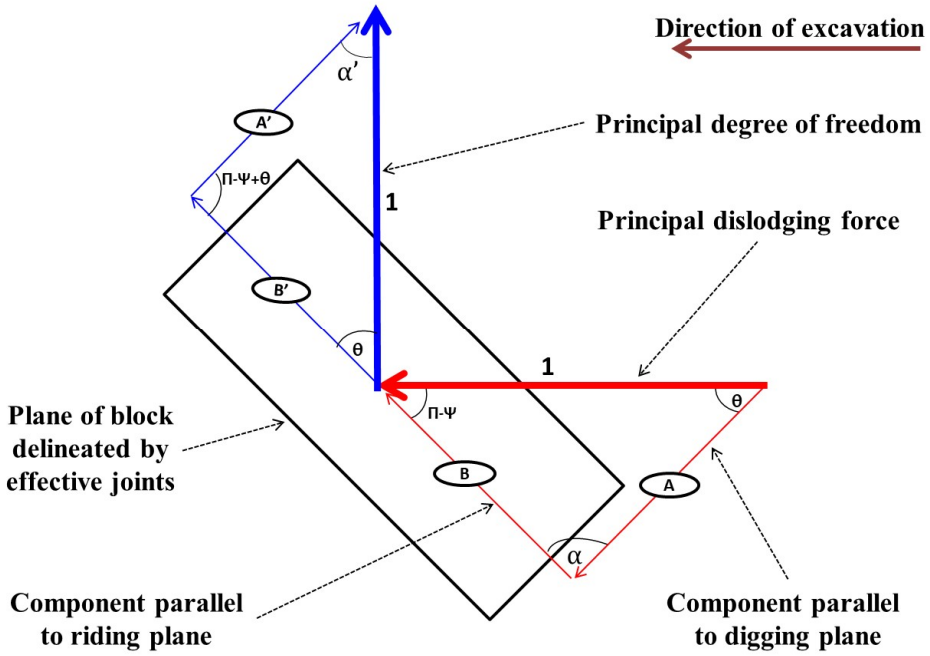

Fig. 3. Representation of the coaxial components as adapted from Kirsten (1982).

The coaxial component, identified as A in Fig. 3, is in the opposite direction of the coaxial component, identified as A' in Fig. 3. Accordingly, K_d can be expressed as a function of the other two coaxial components, identified as B and B' (Fig. 3). These two coaxial components can be determined according to following equation:

$$\left.\begin{aligned} B &= \frac{\sin\theta}{\sin(\psi - \theta)} \\ B' &= \frac{\cos\theta}{\sin(\psi - \theta)} \end{aligned}\right\} \tag{6}$$

Thus, the final equation of K_d is given by the product of the two components of B and B'. This equation is expressed as follows:

$$K_d = \frac{\cos\theta \,.\, \sin\theta}{b \sin^2(\psi - \theta)} \tag{7}$$

The value of b in Eq. (8) is 1 based on empirical assessments of the effects of the direction of ripping on the efficiency of ripping (Kirsten 1982). Furthermore, it is assumed that the sum of

K_d and the required dislodging effort (J_s^d) is equal to 1 ($K_d + J_s^d = 1$). Therefore, J_s^d can be expressed according to Eq. (8):

$$J_s^d = \left[1 - \left| \frac{\cos\theta \,.\, \sin\theta}{b \sin^2(\psi - \theta)} \right| \right] \tag{8}$$

2.3. Relative block structure rating

Eq. (5) and (8) were combined to obtain Eq. (9) representing the product of J_s^p and J_s^d. Eq. (9) has been used to determine the relative block structure rating (Js).

$$J_s = \left[1 - \frac{r \tan\theta + \tan\psi}{a\,(r+1)} \right] . \left[1 - \left| \frac{\cos\theta \,.\, \sin\theta}{b \sin^2(\psi - \theta)} \right| \right] \tag{9}$$

The values of Js were determined by Kirsten (1982) using four values of RJS ($r = S\psi/S\theta$): r of 1:1, 1:2, 1:4 and 1:8 (e.g. 1:2 = 2/1 = 2, where 1 represents the width of the block and 2 represents its length). Beyond a RJS of 8 (1:8), the values of Js do not show any significant change. For this reason, the maximum adopted RJS was $r = 8$. The initial results, derived from Eq. (9), are presented in Table 1. However, published Js values presented by Kirsten (1982) do not generally match the results obtained using Eq. (9). Kirsten graphically represented the results obtained using Eq. (9). He then adjusted the obtained curves to determine, from the final adjusted curves, the Js rating. It should be noted that no determination can be performed when $\theta = 0°$ or 90° as Kirsten considered K_d and K_p to be zero when the joints are sub-horizontal (dip = 0°) or sub-vertical (dip = 90°). For these cases, Kirsten assigned a Js value of 1 for the four values of RJS. Indeed, when K_p and $K_d = 0$, Eq. (9) has Js as the product of $1 \times 1 = 1$, explaining the Js values of 1 when dips are 0° or 90°. For excavatability, Kirsten posits that the ground would not be excavated when $Js = 1$, as the sub-horizontal or sub-vertical joints, relative to the ground surface, would not constitute a situation favorable for excavation.

Table 1. The RJS and the angles θ and Ψ initially used by Kirsten (Kirsten 2016, pers. comm.).

Direction of excavation[1]	θ	Ψ	Ratio of joint spacing			
			1	2	4	8
In the direction of excavation	89	179	-4.64	-6.52	-8.02	-9.02
	85	175	-0.12	-0.47	-0.75	-0.94
	80	170	0.37	0.21	0.08	0.00
	75	165	0.49	0.39	0.31	0.26
	70	160	0.52	0.45	0.39	0.35
	65	155	0.51	0.46	0.42	0.39
	60	150	0.50	0.46	0.42	0.40
	55	145	0.49	0.45	0.42	0.40
	50	140	0.49	0.46	0.43	0.41
	45	135	0.50	0.47	0.44	0.42
	40	130	0.53	0.49	0.46	0.45
	35	125	0.57	0.53	0.50	0.48
	30	120	0.63	0.59	0.55	0.53
	25	115	0.72	0.67	0.62	0.60
	20	110	0.84	0.77	0.71	0.68
	15	105	1.01	0.91	0.83	0.78
	10	100	1.28	1.12	0.99	0.91
	5	95	1.95	1.60	1.32	1.13
	0,5	90,5	12.35	8.56	5.53	3.51
Against the direction of excavation	-5	85	-0.12	0.23	0.51	0.70
	-10	80	0.37	0.54	0.66	0.75
	-15	75	0.49	0.59	0.67	0.72
	-20	70	0.52	0.59	0.64	0.68
	-25	65	0.51	0.57	0.61	0.64
	-30	60	0.50	0.55	0.58	0.60
	-35	55	0.49	0.53	0.56	0.58
	-40	50	0.49	0.52	0.55	0.57
	-45	45	0.50	0.53	0.56	0.58
	-50	40	0.53	0.56	0.59	0.61
	-55	35	0.57	0.61	0.64	0.66
	-60	30	0.63	0.68	0.71	0.73
	-65	25	0.72	0.77	0.82	0.85
	-70	20	0.84	0.91	0.97	1.00
	-75	15	1.01	1.11	1.19	1.24
	-80	10	1.28	1.45	1.58	1.66
	-85	5	1.95	2.30	2.58	2.77
	-89	1	6.61	8.49	9.99	10.99

1: This column was added to better explain the presented concepts.

On the other hand, a ground characterized by a *Js* of 1 would have a representative value of its excavatability being determined according to the factors included in Kirsten's index. However, it is practically non-excavatable. Accordingly, the curve adjusting process was undertaken by considering that the curves must be plotted with a *Js* of 1 when the dip is 0° or 90°. From this, two conditions have been respected during the adjusting of curves. The first condition is imposed to avoid negative determinations of *Js*, and the second condition is imposed to have a constant behavior of the *Js* curves.

Furthermore, when the RJS = 1, joint spacing is of the same order for the two considered joint sets. This means that the length and the width of the blocks are of the same order. For this situation, it is impossible to determine which of the two joint sets represents the closer spaced joint set. Consequently, determining the orientation of the blocks relative to the direction of flow has two possible options: the blocks can be considered as being oriented in or against the direction of flow. The RJS in Fig. 4 is 1. If the first joint set is considered to be the closer spaced joint set, the block is oriented accordingly in the direction of flow (dip angle is 30°). If the second joint set is considered to be the closer spaced joint set, the block is oriented accordingly against the direction of flow (dip angle is 60°). Consequently, when the blocks are oriented in the direction of flow with a dip of 30°, *Js* is of the same order as when the blocks are oriented against the direction of flow with a dip of 60°. This principle, indicated hereinafter as the « same required effort principle », was adopted by Kirsten.

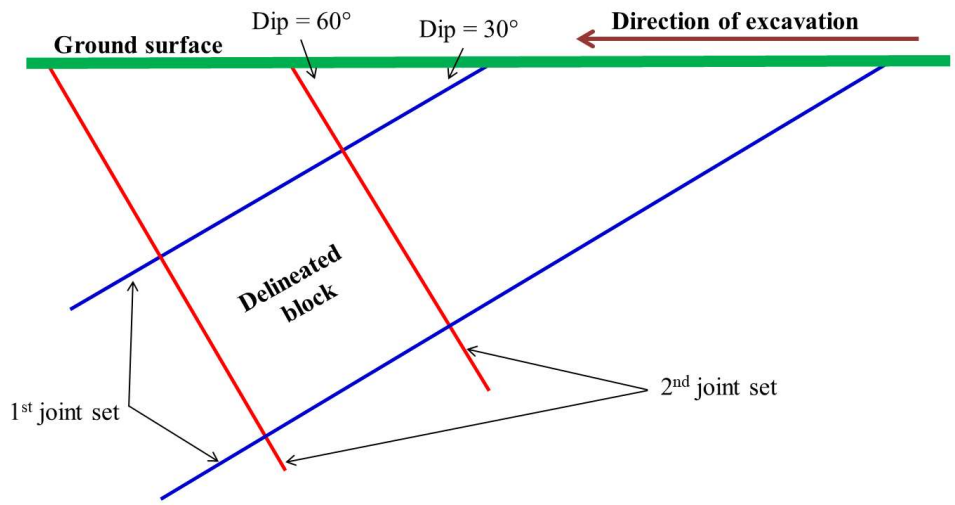

Fig. 4. Orthogonal fractured system with RJS of 1.

The adjustment process, run based on a RJS of 1:1 and 1:8, is presented in Fig. 5 (the adjustment is represented by dashed lines). The final adjusted curves, according to the four RJS, are shown in Fig. 6. For their part, *Js* values determined from these final curves are presented in Table 2 (Kirsten 1982, 1988). Comparing the *Js* values initially proposed by Kirsten (1982, 1988) to evaluate the mechanical excavatability of earth materials and the *Js* values proposed by Annandale (1995, 2006) to evaluate the hydraulic erodibility of earth materials, there are slight differences that likely occurred due to another adjustment process.

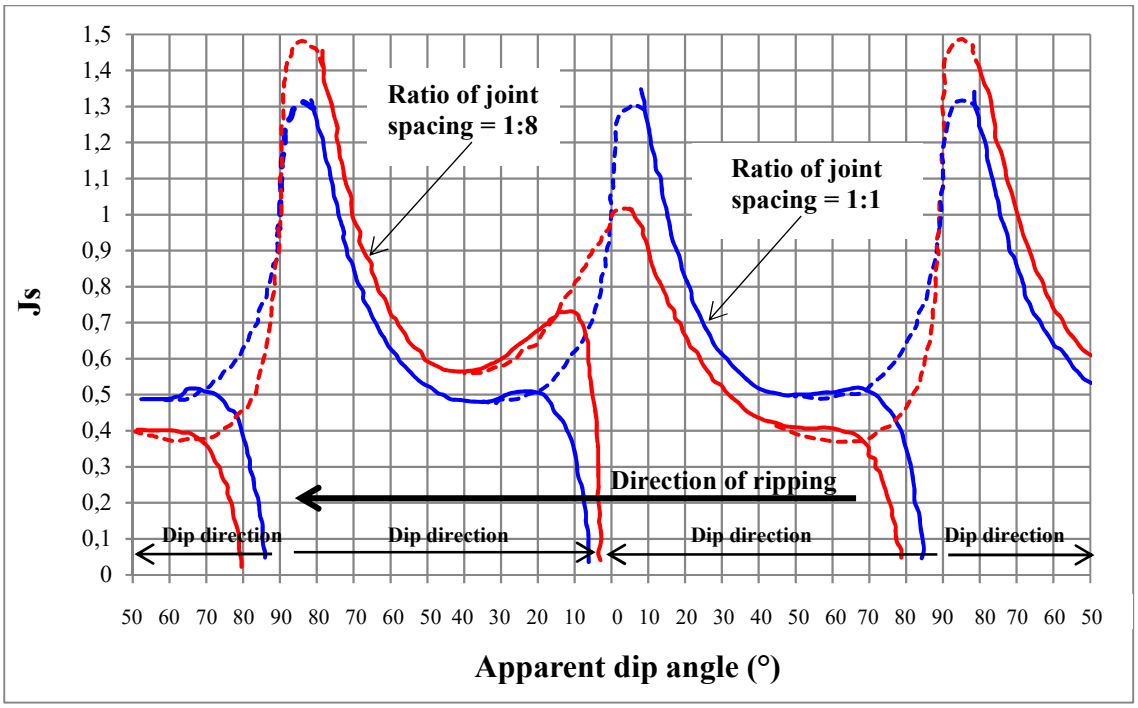

Fig. 5. The curve adjustment process (adapted from Moore and Kirsten 1988).

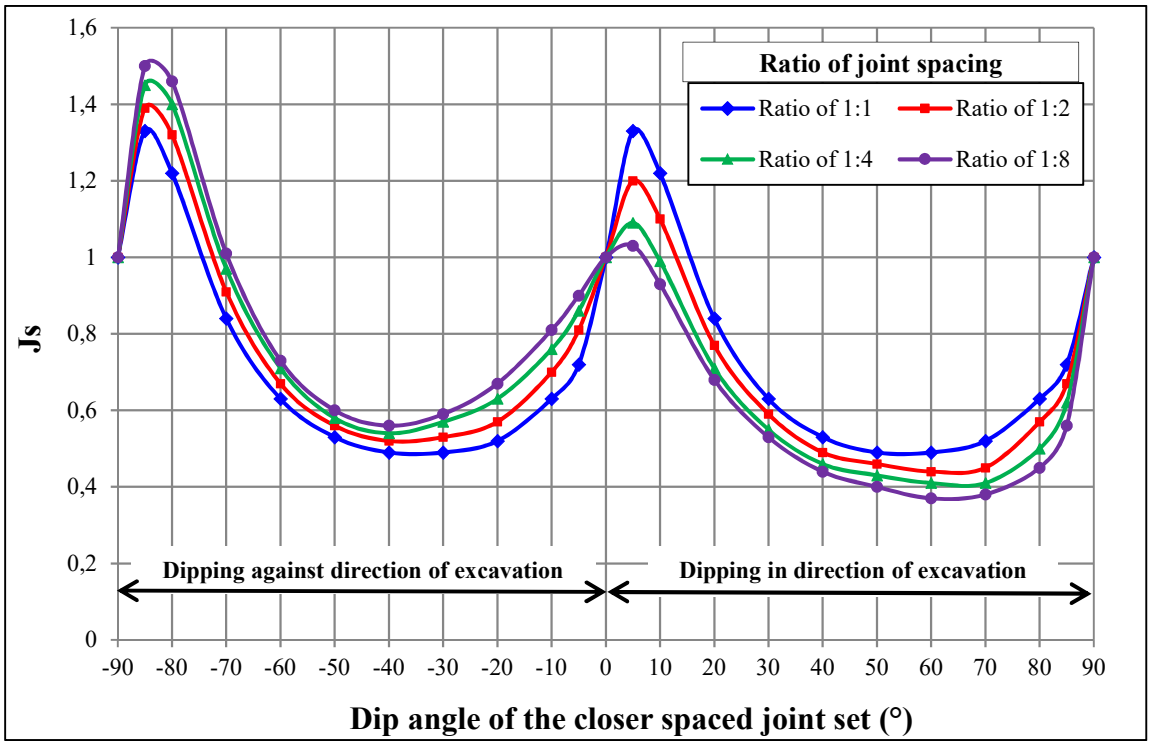

Fig. 6. Graphical representation of the relative block structure values.

Table 2. Rating values of the relative block structure (Kirsten 1982, 1988).

Dip direction[1] of the closer spaced joint set (°)	Dip angle[2] of the closer spaced joint set (°)	Ratio of joint spacing (r)			
		1:1	1:2	1:4	1:8
		Values of relative block structure (Js)			
180/0	90	1	1	1	1
In the direction of excavation	85	0.72	0.67	0.62	0.56
	80	0.63	0.57	0.5	0.45
	70	0.52	0.45	0.41	0.38
	60	0.49	0.44	0.41	0.37
	50	0.49	0.46	0.43	0.4
	40	0.53	0.49	0.46	0.44
	30	0.63	0.59	0.55	0.53
	20	0.84	0.77	0.71	0.68
	10	1.22	1.1	0.99	0.93
	5	1.33	1.2	1.09	1.03
0/180	0	1	1	1	1
Against the direction of excavation	5	0.72	0.81	0.86	0.9
	10	0.63	0.7	0.76	0.81
	20	0.52	0.57	0.63	0.67
	30	0.49	0.53	0.57	0.59
	40	0.49	0.52	0.54	0.56
	50	0.53	0.56	0.58	0.6
	60	0.63	0.67	0.71	0.73
	70	0.84	0.91	0.97	1.01
	80	1.22	1.32	1.4	1.46
	85	1.33	1.39	1.45	1.5
180/0	90	1	1	1	1

1: Dip direction of the closer spaced joint set relative to the direction of excavation
2: Apparent dip of the closer spaced joint set in the vertical plane containing the direction of excavation
3: For intact material, Js = 1
4: For values of r less than 0.125, take Js as for r = 0.125

In practice, the dip angle of the closer spaced joint set and its dip direction relative to the direction of flow are used to determine *Js* values. The dip angle is between 0° and 90°, while the dip direction is determined as a function of the direction of flow. In the example shown in Fig. 7A, the direction of flow is 320°. If the closer spaced joint set has a dip direction between 230° (320° - 90°) and 50° (320° + 90°), it is considered to be in the same direction as that of the flow. Otherwise, it is against direction of flow. If the closer spaced joint set in Fig. 7A is the first joint

set, the dip direction will be taken as being in the direction of flow. Thus, the dip of the closer spaced joint set should be evaluated to determine the *Js* value. Kirsten (1982) considered the geological formation to be fractured by an orthogonal system. Thus, he always maintained an angle of 90° between the planes of the two joint sets (this angle is indicated hereinafter as α). It should be noted that this situation only occurs when the direction of flow is perpendicular to the azimuth of the closer spaced joint set. If the direction of flow is not perpendicular, Kirsten suggests taking the apparent dip of the closer spaced joint set, in the vertical plane containing the direction of flow, to determine the *Js* value (Table 2).

In Fig. 7A, the two joint sets constitute an orthogonal fractured system. The dip and dip direction of the first joint set are 30° and 270°, respectively; those of the second joint set are 60° and 90°, respectively. The first joint set is considered as the closer spaced joint set, and the direction of flow is 320°. The apparent dip used to determine *Js* would therefore be 20°. However, it is found that α, on the plane containing the direction of flow, is 112° (Fig. 7A). Remembering that the *Js* value, when the dip is 20°, was initially proposed by Kirsten with α = 90° (orthogonal fractured system), it does not seem appropriate to only consider the apparent dip in such situations. The change of the angle between the joint sets along the vertical plane containing the direction of flow should also be considered. Such a situation, where α differs from 90° (on the vertical plane containing the direction of flow), is equivalent to a flow having a direction that is perpendicular to the strike of the closer spaced joint set, but in a non-orthogonal fractured system as shown in Fig. 7B. For this situation, the first joint set has a dip of 20°, while the dip of the second joint set is 48°. Our work aims to determine the *Js* rating for non-orthogonal fractured systems, which includes the *Js* rating when the direction of flow is not perpendicular to the azimuth of the closer spaced joint set.

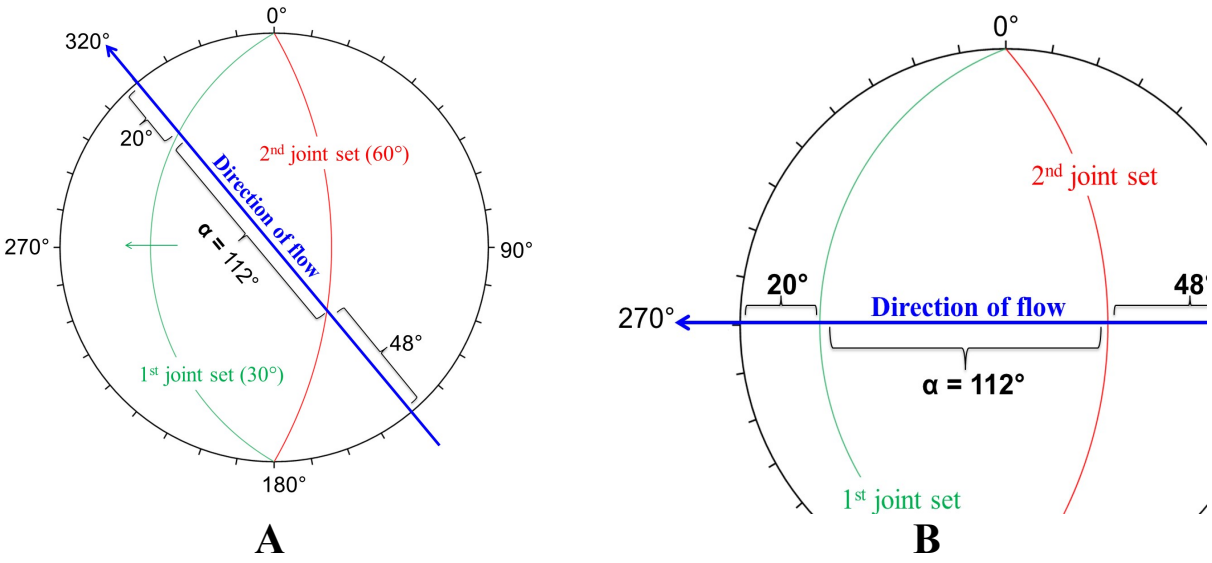

Fig. 7. Stereographic representation of two possible situations for a fractured system.

3. Methodology

As already mentioned, the block dislodging action is controlled by K_p and K_d, while the α angle for non-orthogonal fractured systems could be larger or smaller than 90°. Kirsten's *Js* equation (Eq. 9) could be used for this purpose. However, his initial relative block structure concept must be adjusted. As a modification of α angle in the equation for K_d subsequently modifies the equation for K_p, only K_d is adjusted. This section describes the principle of the adjusted relative block structure concept that is used to develop a new set of equations for determining K_d. These new equations are then included as part of the equation for *Js* to propose a rating of *Js* for non-orthogonal fractured systems.

3.1. Principle of the adjusted concept

The RJS values, as well as angles θ and Ψ initially used by Kirsten to determine *Js* values, are presented in Table 1. Based on this data, a representation of two blocks is shown in Fig. 8. The planes of the joints associated with θ and Ψ are plotted in blue and red, respectively (Fig. 8).

When the block is oriented in the direction of excavation, Kirsten considered θ to be positive (e.g. θ = 30°), while the Ψ is determined by adding an angle of 90° to θ (e.g. θ = 30°, thus Ψ = 30° + 90° = 120°). On the other hand, when the block is oriented against the direction of excavation, Kirsten considered θ to be negative (e.g. θ = -30°), while Ψ is determined by again adding an angle of 90° to θ (e.g. θ = -30°, thus Ψ = -30° + 90° = 60°). For these two orientations of block relative to direction of excavation, Kirsten always kept α = 90° between the planes of the joints associated to θ and Ψ to consider this as an orthogonal fractured system.

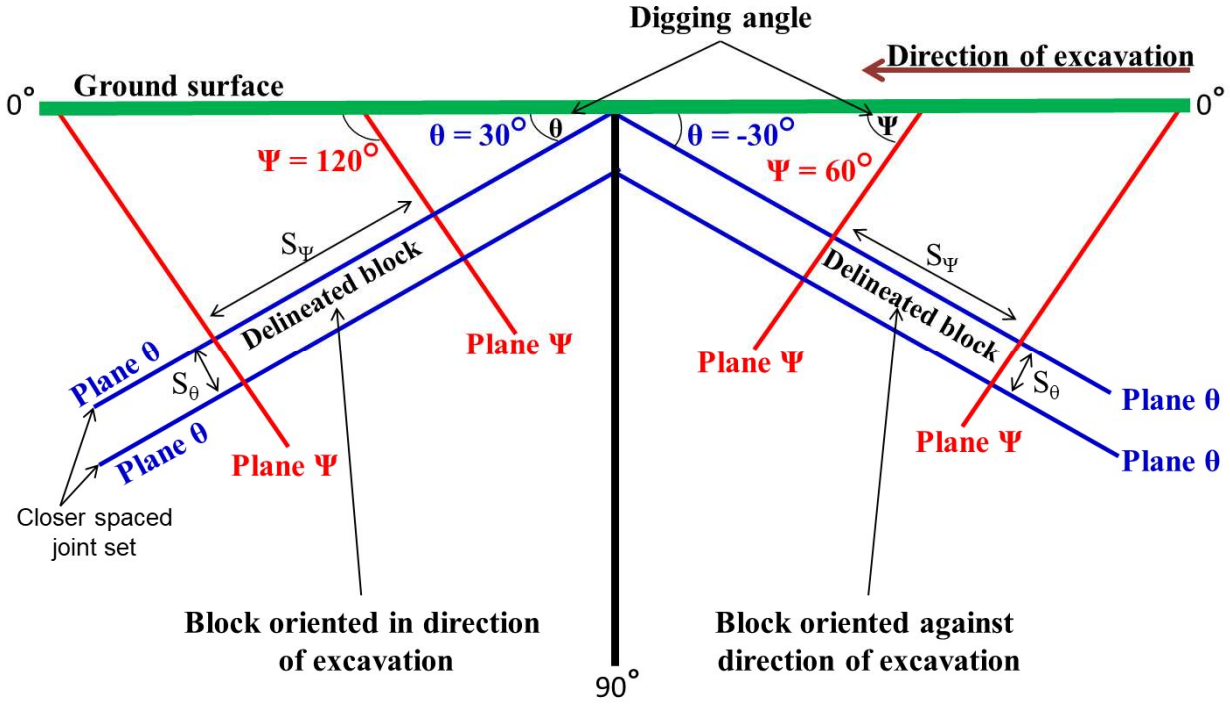

Fig. 8. Concept of a delineated block oriented in and against the direction of excavation.

Based on the concept presented in Fig. 8, when the block is oriented in or against the direction of excavation, the joint spacing S_Ψ is always greater than the joint spacing S_θ. Therefore, the RJS (S_Ψ/S_θ) is of the same order for both blocks, although their orientations differ (Fig. 8). This explains why Kirsten always used the same fixed RJS (1 = 1:1, 2 = 1:2, 4 = 1:4, 8 = 1:8) for both directions of the block (in the direction of excavation and against the direction of

excavation). On the other hand, Kirsten's initial representation, as shown in Fig. 1 where a block is oriented against the direction of excavation, the joint spacing S_Ψ is smaller than the joint spacing S_θ. For this, the corresponding RJS should not be of the same order as that presented in Table 1. If, for example, $S_\Psi = 1$ and $S_\theta = 2$, the RJS would be 1/2 = 0.5. In addition, Note 4 in Table 2 states that for an RJS >0.125, *Js* is determined as if the RJS = 0.125. This value of 0.125 represents the ratio of 1/8, rather than 8/1 as presented in Table 1. The value of 0.125 has also been noted by Kirsten (1988) and the USDA (1997). Annandale (1995, 2006) has corrected this by indicating that beyond a RJS of 8 (1:8 = 8/1 = 8), *Js* could be considered as having a RJS of 8. However, the initial concept presented in Fig. 1 could be adjusted. Indeed, when the block is oriented against the direction of excavation, the digging angle is Ψ (Fig. 8), while Kirsten (1982) represents this angle, as shown in Fig. 1, as θ. Given that the two coaxial components considered for K_d are obtained having the digging angle as θ (Section 2.1), the equation of K_d (Eq. 7) presented by Kirsten (1982) must be adjusted if the digging angle is considered to be Ψ (Fig. 8). This is also taken into account when the block is oriented in the direction of excavation. Indeed, the digging angle for this situation would be the θ (Fig. 8). Consequently, two equations of K_d will be proposed according to the adopted digging angles.

Furthermore, it should be noted that the orientation of the block can be changed depending on the rotation center being the convergence point between the principal dislodging force and the principal degree of freedom (Fig. 9). The concept of the principal dislodging force and the principal degree of freedom can be seen as being the same concept for a block oriented in and against the direction of excavation as shown in Fig. 9. Therefore, the two components of opposite directions (identified A and A' in Fig. 9) will not be considered, whatever the orientation of the

block, and consequently K_d will be determined according to the other coaxial components, those identified B and B' in Fig. 9.

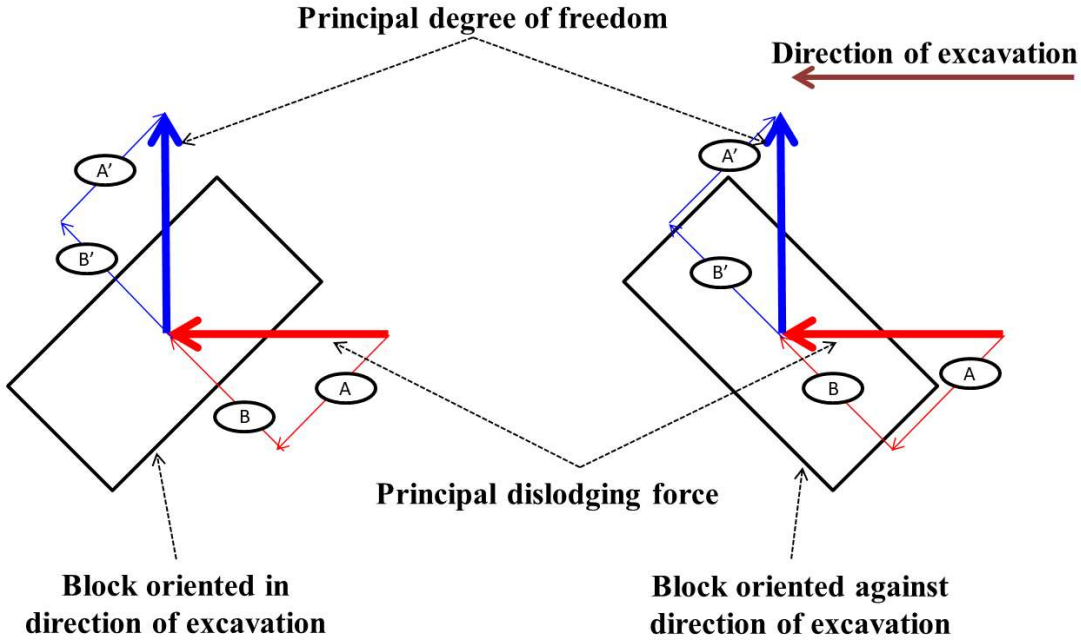

Fig. 9. Coaxial components for blocks oriented in and against the direction of excavation.

3.2. Proposed K_d equation when the block is oriented in direction of flow

The concept of a block oriented in direction of flow is shown in Fig. 10. According to the determination of the coaxial components of the principal dislodging force and the principal degree of freedom for a block oriented in the direction of flow (Fig. 10), the unknown angle (considered as α), as well as the coaxial components (B) and (B') can be determined according to the following:

$$\left.\begin{aligned} \alpha &= \psi - \theta \\ B &= \frac{\sin\theta}{\sin(\psi - \theta)} \\ B' &= \frac{\sin(\frac{\pi}{2} - \theta)}{\sin(\psi - \theta)} \end{aligned}\right\} \quad (10)$$

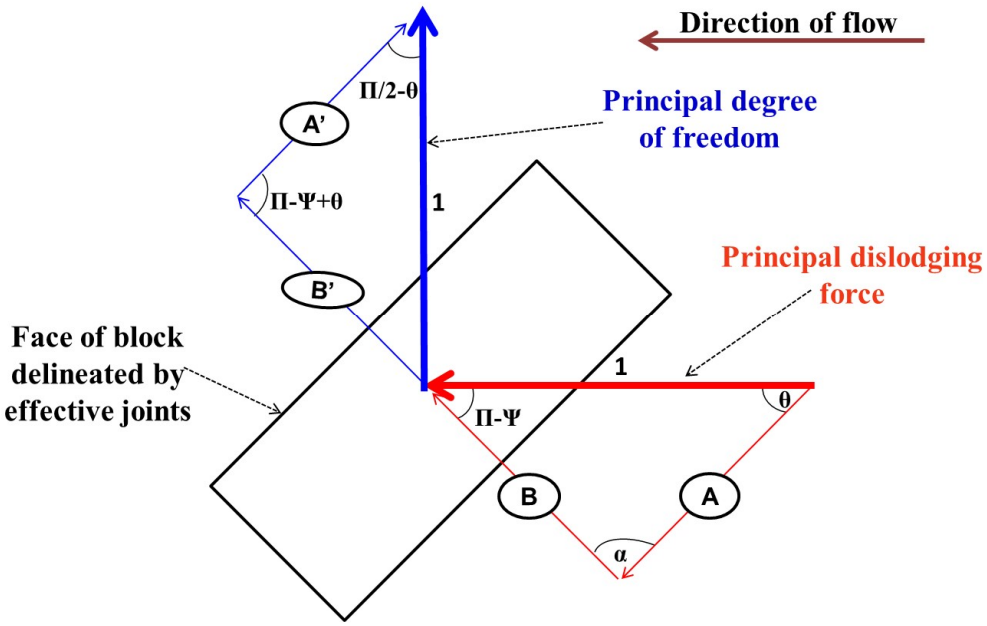

Fig. 10. Coaxial components for a block oriented in the direction of flow.

The final equation of K_d when the block is oriented in the direction of flow is given by the product of the two components B and B'. This final equation is expressed as follows:

$$K_d = \frac{\sin\theta \,.\, \cos\theta}{\sin^2(\psi - \theta)} \tag{11}$$

It should be mentioned that Eq. (11) can be applied under the following conditions:

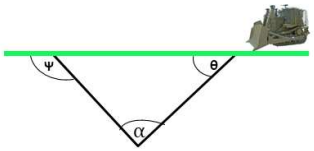

$$\rightarrow \quad \left.\begin{array}{c} \psi = \alpha + \theta \\ 0° < \theta < 90° \\ 90° < \psi < 180° \end{array}\right\} \tag{12}$$

3.3. Proposed K_d equation when the block is oriented against direction of flow

The concept of a block oriented against the direction of flow is shown in Fig. 11. According to the determination of the coaxial components of the principal dislodging force and the principal degree of freedom for a block oriented in the direction of flow (Fig. 11), the unknown angle (considered as α) and the coaxial components (B) and (B') could be determined according to following expressions:

$$\left.\begin{aligned} \alpha &= \theta - \psi \\ B &= \frac{\sin \psi}{\sin\ (\theta - \psi)} \\ B' &= \frac{\sin\ (\frac{\pi}{2} - \psi)}{\sin (\theta - \psi)} \end{aligned}\right\} \qquad (13)$$

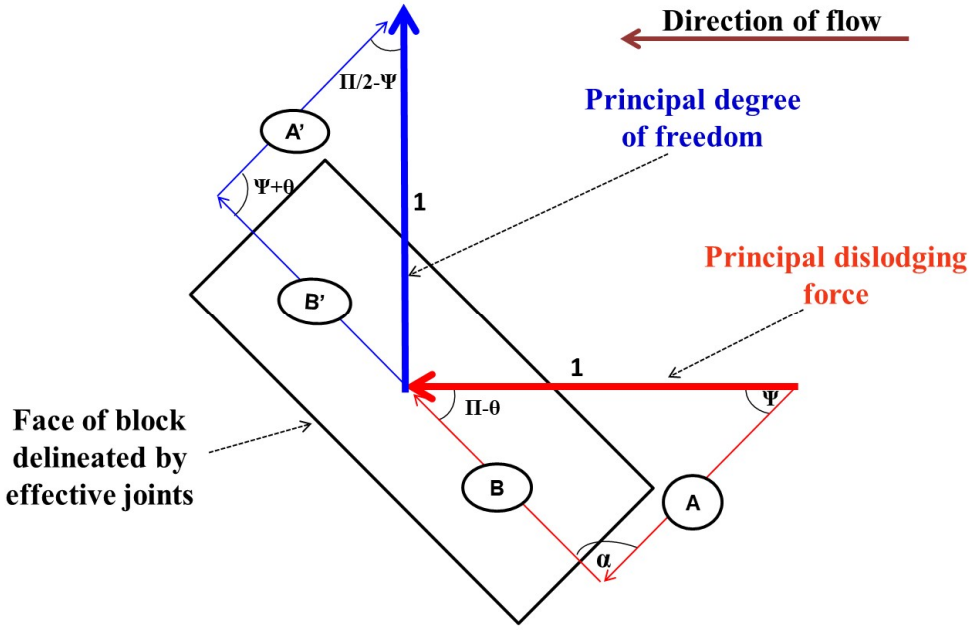

Fig. 11. Coaxial components for a block oriented against the direction of flow.

The final equation of K_d when the block is oriented against the direction of flow is given by the product of the two components B and B'. This final equation is expressed as follows:

$$K_d = \frac{\sin \psi \,.\, \cos \psi}{\sin^2 (\theta - \psi)} \qquad (14)$$

It should be mentioned that Eq. (14) can be applied under the following conditions:

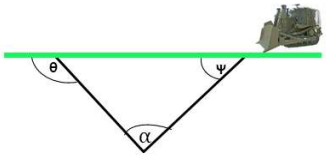

$$\rightarrow \qquad \left.\begin{aligned} \psi &= \theta - \alpha \\ 90° &< \theta < 180° \\ 0° &< \psi < 90° \end{aligned}\right\} \qquad (15)$$

3.4. *Analysis of K_d behavior*

The behavior of K_d is assessed according to Eqs. (11) and (14) that represent K_d when the block is oriented in and against the direction of flow, respectively. The results for K_d are shown in Fig. 12. For blocks oriented against the direction of flow, θ is represented as dips ranging from 0° to 90°. Thus, for example a θ = 175° used for the calculating K_d is represented on the curve as an angle of 5°. According to Fig. 12, K_d presents the same behavior when the block is oriented in or against the direction of flow. Since the orientation of the block changes depending on the rotation center, the concept of the principal dislodging force and the principal degree of freedom is always maintained regardless of the block's orientation relative to the direction of flow. Thus K_d, for the same dip, is of the same value when the block is oriented in or against the direction of flow. This is confirmed by the proposed equations.

The results obtained from the proposed equations are in perfect agreement with results obtained through Kirsten's concept. Thus, the proposed equations provide reliable estimates of K_d without these equations being forced to be expressed in absolute terms, as proposed by Kirsten (1982). It should be noted that the K_d values determined according to Kirsten's concept, when the block is oriented against or in direction of excavation, are not equal as shown in Fig. 13. For example, K_d = -0.09 for a dip θ = 5° oriented against the direction of excavation, while it is 0.09 for a dip θ = 5° oriented in the direction of excavation. Consequently, Kirsten expresses K_d in absolute terms (Eq. 8) and produced identical K_d values when the block is oriented in or against the direction of excavation.

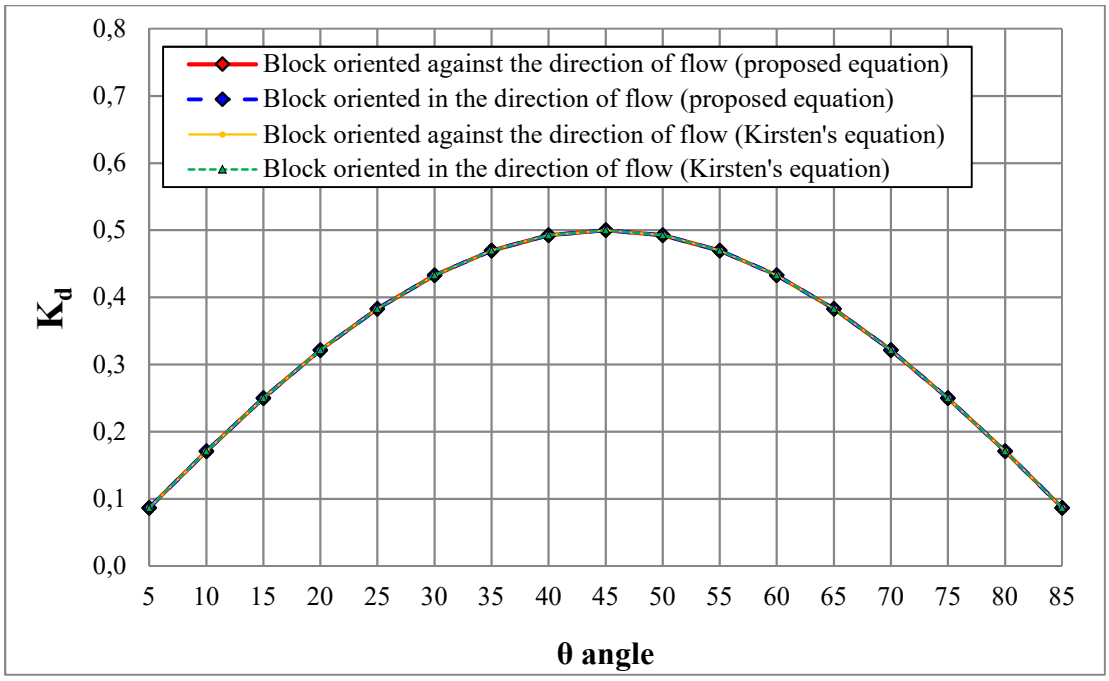

Fig. 12. Behavior of the kinematic possibility of dislodgment versus θ.

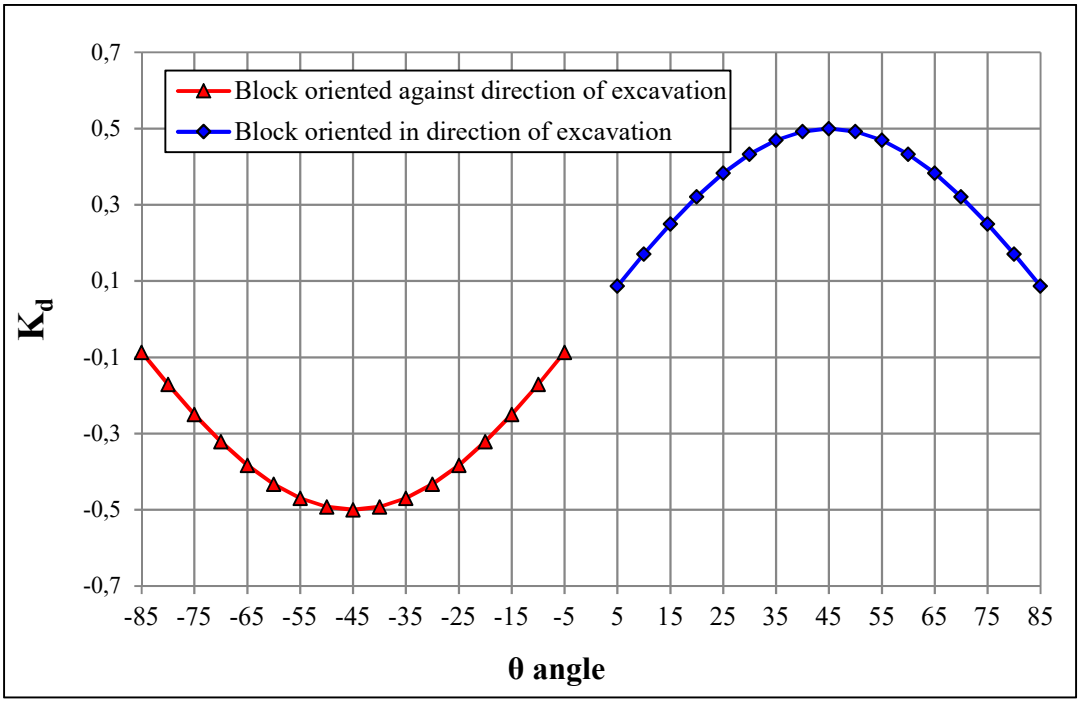

Fig. 13. Behavior of the kinematic possibility of dislodgment not expressed in absolute terms.

3.5. *Proposed equations for determining Js*

Considering that the required effort is equal to 1 minus the kinematic possibility as proposed by Kirsten (1982), *Js* values can be determined by the proposed Eqs. (16) and (17). Eq. (16) is applied when the blocks are oriented in the direction of flow (Eq. 11 for K_d is introduced), while Eq. (17) is used when the blocks are oriented against the direction of flow (Eq. 14 for K_d is introduced). It should be noted that no change is introduced to the equation for K_p (Eq. 4).

$$J_s = \left[1 - \frac{r \tan\theta + \tan\psi}{a\,(r+1)} \right] . \left[1 - \frac{\sin\theta \,.\, \cos\theta}{\sin^2(\psi - \theta)} \right] \tag{16}$$

$$J_s = \left[1 - \frac{r \tan\theta + \tan\psi}{a\,(r+1)} \right] . \left[1 - \frac{\sin\psi \,.\, \cos\psi}{\sin^2(\theta - \psi)} \right] \tag{17}$$

4. Results and discussion

Determining *Js* values for the non-orthogonal fractured systems is carried out according to the proposed Eqs. (16) and (17) using a RJS of 1, 2, 4 and 8 for the case of blocks oriented in and against the direction of flow. It should be noted that when θ = 0°, 90° and 180°, the *Js* value is 1 (Section 2.3). Therefore, no analyses are performed for these angles.

4.1. *Determining Js when α is larger than 90°*

For non-orthogonal fractured systems, α may be > 90° (from 91° to 179°). To determine the role of α > 90° on *Js*, a series of angles are evaluated (100°, 110°, 120°, 130°, 140° and 150°). In geomechanics, planes are usually considered as parallel when the angle between the planes is <20°. Examples of this include the angle between the joint's dip direction and the direction of excavation when determining the orientation factor in the rock mass classification system (RMR) of Bieniawski (1989) and the angle of the joint's dip direction and the direction of slope surface during the analysis of possible planar failure (Wyllie and Mah, 2004). Consequently, α angle for non-orthogonal fractured systems is limited to a maximum of 150°.

The behavior of *Js* as a function of θ (considered as the dip of the closer spaced joint set) when α = 100°, 110°, 120°, 130°, 140° and 150° is shown in Fig. 14. When the block is oriented in the direction of flow, θ ranges from 0° to 90° whereas θ ranges from 90° to 180° when the block is oriented against the direction of flow (Eq. 14). However, the latter angles are represented as angles varying from 0° to 90° marked by a negative sign. For example, a θ = 150° corresponds to an angle of 30° (θ = 180° - 150°) in Fig. 14.

When α = 100° (Fig. 14A), *Js* is not calculated for a θ ≥ 80°. This is explained by a non-favorable geometry applying to the conditions as indicated in Eqs. (12) and (15). Similar situations are noted with the pairings α = 110° and θ ≥ 70° (Fig. 14B), α = 120° and θ ≥ 60° (Fig. 14C), α = 130° and θ ≥ 50° (Fig. 14D), α = 140° and θ ≥ 40° (Fig. 14E) and α = 150° and θ ≥ 30° (Fig. 14F). Moreover, when α = 100°, 110°, 120° and 130°, the *Js* behavior curves vary according to the RJS. However, when α = 140° or 150°, the *Js* behavior curves do not vary with the RJS. Thus, the RJS has no effect when α > 130°. Accordingly, the proposed *Js* values can be assigned for any RJS when α = 140°. This process is also valid when α = 150°.

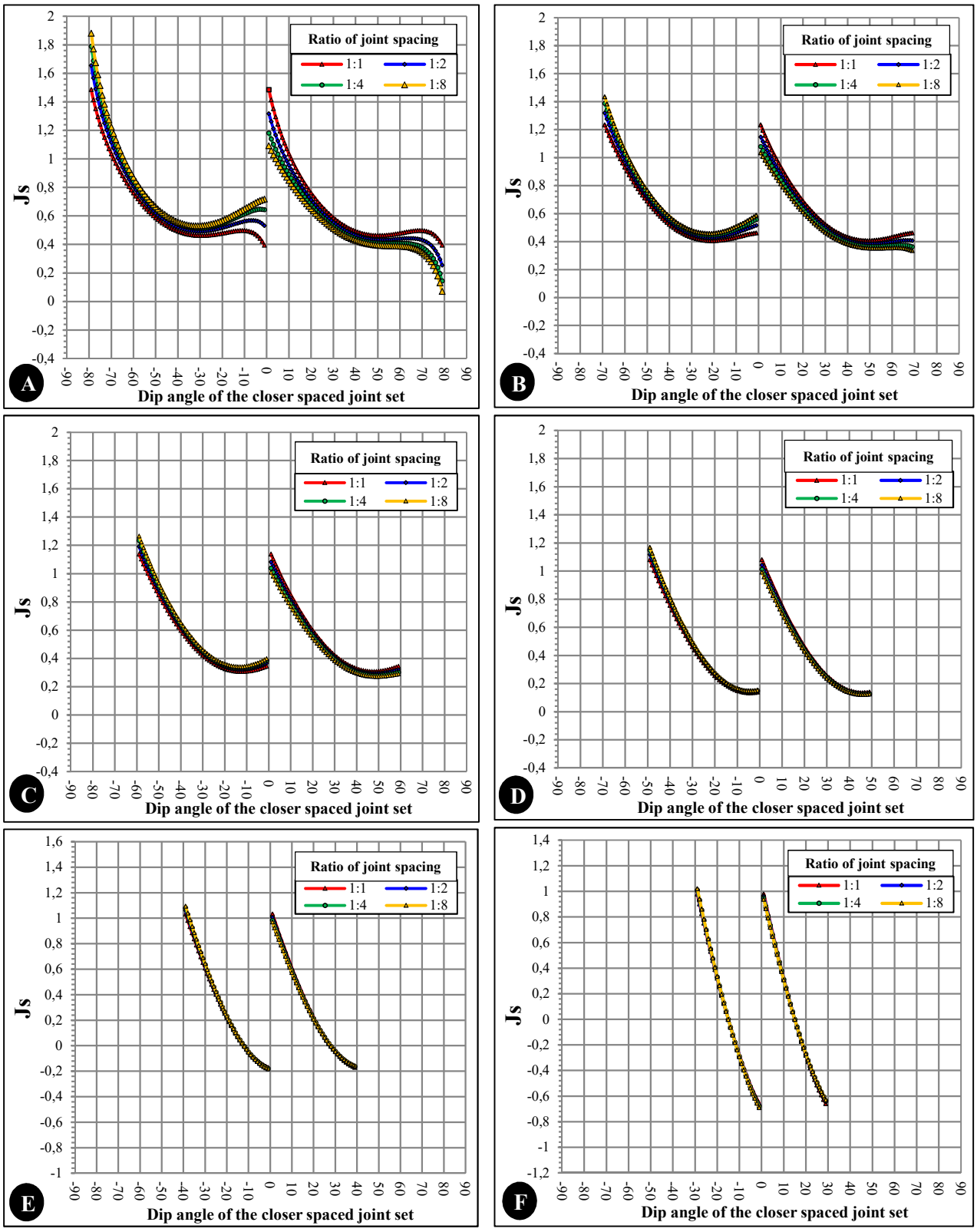

Fig. 14. Behavior of *Js*: A) α = 100°, B) α = 110°, C) α = 120°, D) α = 130°, E) α = 140°, F) α = 150°.

Although the dip of the closer spaced joint set can vary from 0° to 90°, to keep the same considerations as Kirsten (1982), only dip angles used by Kirsten (1982) are used in the adjustment process. These dips correspond to 5°, 10°, 20°, 30°, 40°, 50°, 60°, 70°, 80°, 85° and 90°. Moreover, the adjustment process is performed for a RJS of 1, 2, 4 and 8. However, only the adjustment process followed for a RJS of 8 is discussed in this paper. For the other RJS, the same method is applied.

When the blocks are oriented in the direction of flow, the initial results using Eq. (16) are represented in Fig. 15A; results for blocks oriented against the direction of flow, derived from Eq. (17), are represented in Fig. 15B. Adopting the same adjusting method as Kirsten (explained in Section 2.3), the curve adjusting process considers that the all curves must be plotted with *Js* of 1 when the dip = 0° and 90°. On the other hand, the adjusting process is performed to avoid having negative determinations of *Js*, as exemplified by the Dip/α pairing of 30°/140° where the *Js* value is modified from -0.04 to 0.11 (Fig. 15A and 15C) or the pairing of 5°/140° where the *Js* value is modified from -1.15 to 0.11 (Fig. 15B and 15D). Furthermore, as it is considered that the *Js* values can be of the same order for a given dip, regardless of the RJS when α is = 140° or 150°, the « same required effort principle » is applied during the adjustment process as when a RJS of 1 is used. Thus, in the case of α = 140°, the same required effort principle is applied for a dip of 20° oriented in or against the direction of flow. In the case of α = 150°, the same required effort principle is applied for the dip pairings of 20°/10 and 10°/20° (the first dip of each pairing is oriented in the direction of flow, and the second dip is oriented against the direction of flow). The final adjusted curves when the blocks are oriented in and against the direction of flow are shown in Figs. 15C and 15D, respectively. The final adopted *Js* values are presented in Table 3.

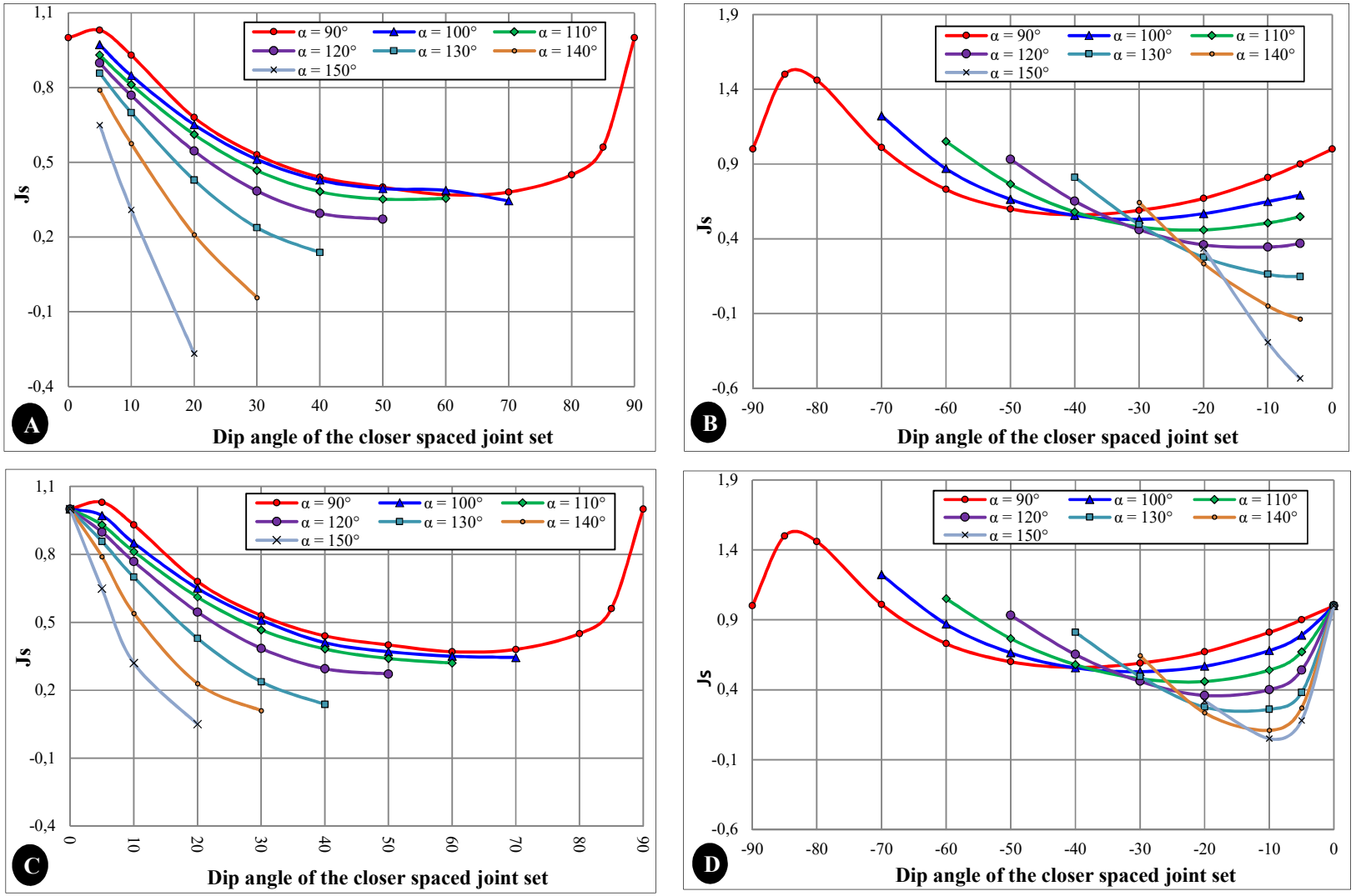

Fig. 15. *Js* curves when RJS = 8: A) Before adjustment-in the direction of flow; B) Before adjustment-against the direction of flow; C) After adjustment-in the direction of flow; D) After adjustment-against the direction of flow.

Table 3. Rating values of relative block structures for a non-orthogonal fractured system (α > 90°).

	Angle of the closer spaced joint set[1]	Angle between the two planes (α)																	
		100°				110°				120°				130°				140°	150°
		Ratio of joint spacing (*r*)																For any *r*	For any *r*
		1:1	1:2	1:4	1:8	1:1	1:2	1:4	1:8	1:1	1:2	1:4	1:8	1:1	1:2	1:4	1:8		
Dip direction of the closer spaced joint set is in the direction of flow	70°	0.50	0.42	0.38	0.34	-	-	-	-	-	-	-	-	-	-	-	-	-	-
	60°	0.46	0.41	0.38	0.35	0.42	0.37	0.35	0.32	-	-	-	-	-	-	-	-	-	-
	50°	0.46	0.42	0.40	0.37	0.41	0.38	0.36	0.34	0.31	0.29	0.28	0.27	-	-	-	-	-	-
	40°	0.49	0.45	0.43	0.41	0.43	0.41	0.39	0.38	0.33	0.31	0.30	0.30	0.15	0.14	0.14	0.14	-	-
	30°	0.59	0.55	0.52	0.51	0.52	0.50	0.48	0.47	0.42	0.41	0.39	0.38	0.26	0.25	0.24	0.24	0.11	-
	20°	0.76	0.71	0.67	0.65	0.69	0.66	0.63	0.61	0.60	0.58	0.56	0.55	0.46	0.45	0.44	0.43	0.23	0.05
	10°	1.04	0.99	0.91	0.85	0.93	0.90	0.84	0.81	0.85	0.82	0.79	0.77	0.76	0.73	0.71	0.70	0.54	0.32
	5°	1.24	1.13	1.03	0.97	1.09	1.02	0.97	0.93	0.99	0.96	0.92	0.90	0.93	0.90	0.87	0.86	0.79	0.65
Dip direction of the closer spaced joint set is against the direction of flow	5°	0.68	0.72	0.75	0.79	0.56	0.60	0.63	0.67	0.44	0.48	0.51	0.54	0.29	0.31	0.34	0.38	0.27	0.18
	10°	0.50	0.60	0.64	0.68	0.42	0.48	0.50	0.54	0.31	0.36	0.36	0.40	0.15	0.21	0.22	0.26	0.11	0.05
	20°	0.46	0.52	0.55	0.57	0.41	0.43	0.45	0.46	0.33	0.34	0.35	0.36	0.26	0.26	0.27	0.28	0.23	0.32
	30°	0.46	0.49	0.51	0.53	0.43	0.45	0.47	0.48	0.42	0.44	0.45	0.46	0.46	0.48	0.49	0.50	0.64	-
	40°	0.49	0.52	0.54	0.56	0.52	0.55	0.57	0.58	0.60	0.62	0.64	0.65	0.76	0.78	0.80	0.81	-	-
	50°	0.59	0.62	0.65	0.66	0.69	0.72	0.75	0.77	0.85	0.89	0.91	0.93	-	-	-	-	-	-
	60°	0.76	0.81	0.84	0.87	0.93	0.98	1.02	1.05	-	-	-	-	-	-	-	-	-	-
	70°	1.04	1.12	1.18	1.22	-	-	-	-	-	-	-	-	-	-	-	-	-	-

1: Apparent dip angle of the closer spaced joint set in a vertical plane containing direction of flow

4.2. *Determining Js when α is less than 90°*

A series of α angles (30°, 40°, 50°, 60°, 70° and 80°) are adopted to evaluate the *Js* rating when α is less than 90°. Cases where α is 10° and 20° are excluded as they represent situations where the planes of the joints are parallel (Bieniawski 1989). The behavior of *Js* with α = 80°, 70°, 60°, 50°, 40° and 30° are presented in Fig. 16. The θ angles in these figures, which originally varied from 90° to 180° (Eq. 14) when the block is oriented against the direction of flow, are represented by an angle varying from 0° to 90° with a negative sign.

When α = 80° and θ = 10° (Fig. 16A), the *Js* value was not determined as the Eqs. (16) and (17) generate aberrant values through use of a Ψ angle of 90° as α = 80° and θ = 10°. Such a situation occurred also for the α/θ pairings of 70°/20° (Fig. 16B), 60°/30° (Fig. 16C), 50°/40° (Fig. 16D), 40°/50° (Fig. 16E) and 30°/60° (Fig. 16F). On the other hand, when α = 80° and θ < 10°, the *Js* value was not valid as the Ψ angle here would have a value beyond that of the validated tuned interval (see the application conditions of Eqs. (12) and (15)). Such a situation also occurred for the α/θ pairings of 70°/<20° (Fig. 16B), 60°/<30° (Fig. 16C), 50°/<40° (Fig. 16D), 40°/<50° (Fig. 16E) and 30°/<60° (Fig. 16F). According to Fig. 16, *Js* curves vary as a function of RJS, except for those at α = 30° (Fig. 16F). Thus, the RJS has no impact when α = 30°.

The outcomes for *Js* when the blocks are oriented against the direction of flow are presented in Fig. 17A, while *Js* values when the blocks are oriented in the direction of flow are shown in Fig. 17B. It should be mentioned that the obtained curves are based on the same adjustment process as Kirsten's (explained in Section 2.3). The curve adjustment process is undertaken 1) to ensure that all curves are plotted with *Js* = 1 when the dip = 0° or 90° and 2) to avoid negative determinations of *Js*, as exemplified by the dip/α pairing of 80°/30° where the *Js*

value of -0.56 (see Fig. 17B) is modified to 0.14 (see Fig. 17D). Furthermore, the « same required effort principle » is applied during the adjustment process, as demonstrated by the dip angle of 70° oriented in the direction of flow and a dip angle of 80° oriented against the direction of flow (and vice-versa). The final adjusted curves when the blocks are oriented in and against the direction of flow are shown in Fig. 17C and 17D, respectively. For their part, the final adopted *Js* values are presented in Table 4.

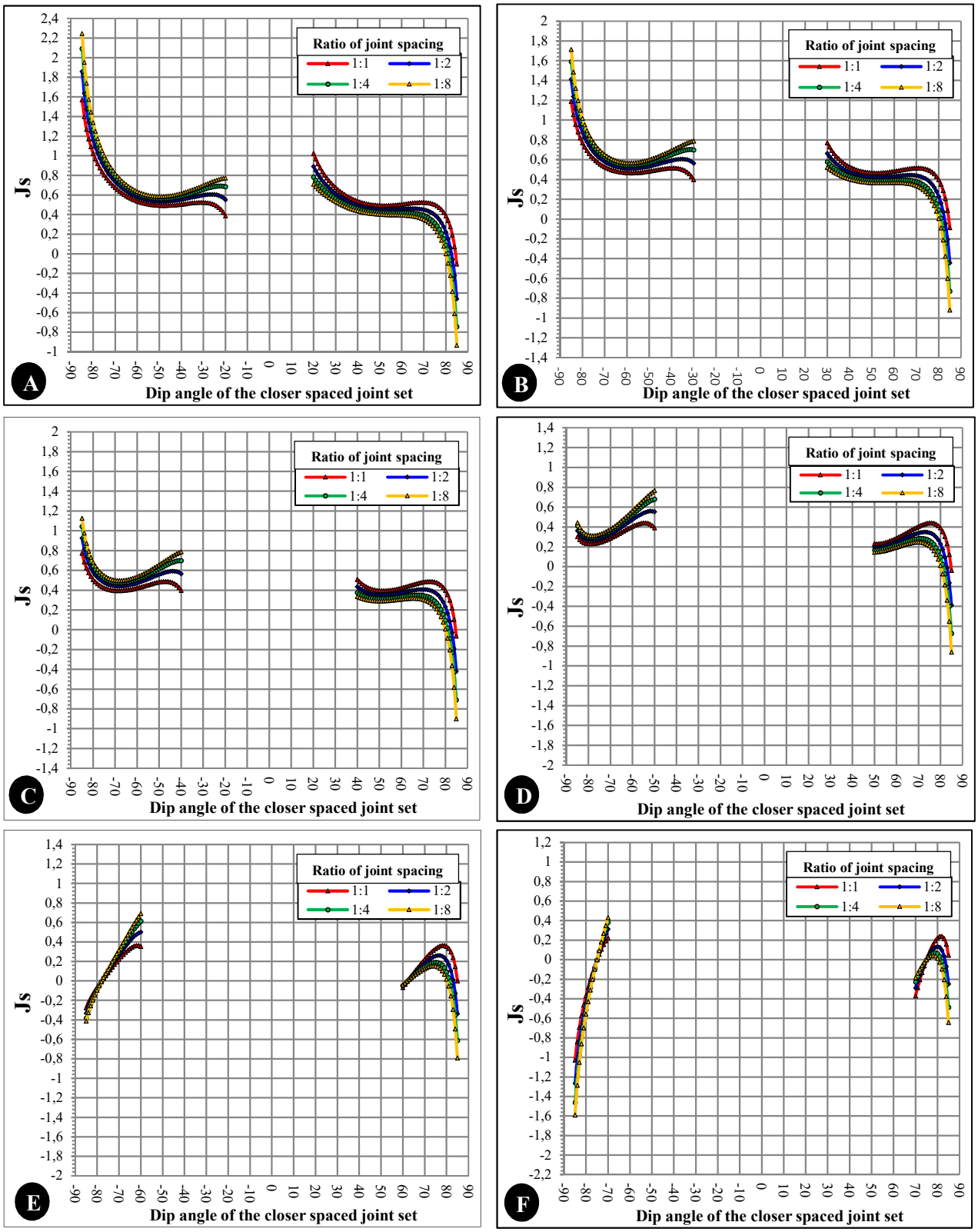

Fig. 16. Behavior of *Js*: A) α = 80°, B) α = 70°, C) α = 60°, D) α = 50°, E) α = 40°, F) α = 30°.

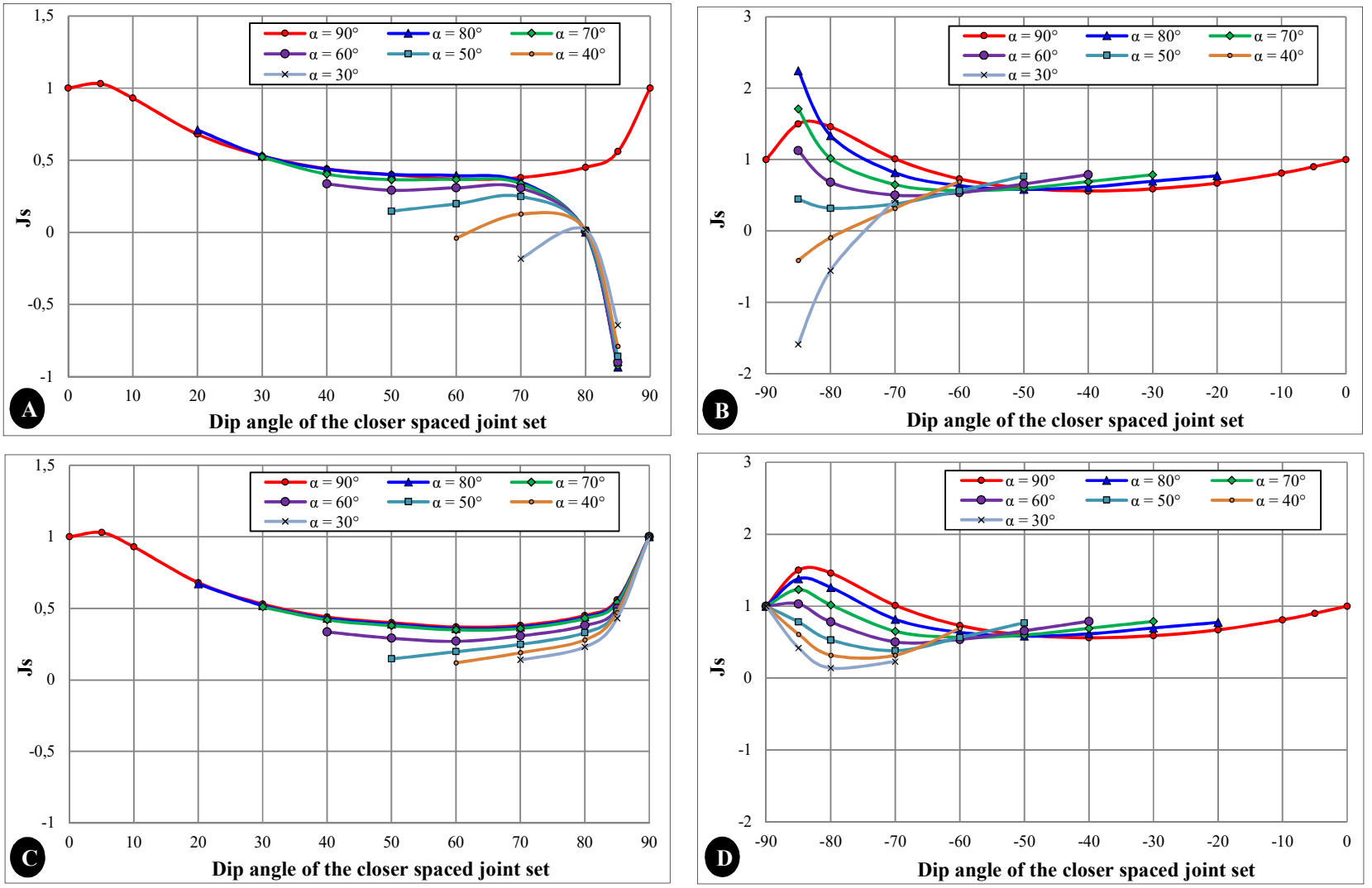

Fig. 17. *Js* curves when RJS = 8: A) Before adjustment-in the direction of flow; B) Before adjustment-against the direction of flow; C) After adjustment-in the direction of flow; D) After adjustment-against the direction of flow

Table 4. Rating values of relative block structures for a non-orthogonal fractured system (α < 90°).

	Angle of closer spaced joint set[1]	Angle between the two planes (α)																			
		80°				70°				60°				50°				40°				30°
		Ratio of joint spacing (*r*)																				For any *r*
		1:1	1:2	1:4	1:8	1:1	1:2	1:4	1:8	1:1	1:2	1:4	1:8	1:1	1:2	1:4	1:8	1:1	1:2	1:4	1:8	
Dip direction of the closer spaced Joint set is in the direction of flow	85°	0.71	0.66	0.61	0.55	0.70	0.65	0.60	0.54	0.63	0.59	0.55	0.50	0.54	0.52	0.50	0.48	0.44	0.45	0.46	0.47	0.43
	80°	0.62	0.56	0.49	0.44	0.61	0.55	0.48	0.43	0.54	0.48	0.44	0.38	0.42	0.42	0.38	0.33	0.27	0.26	0.27	0.28	0.23
	70°	0.51	0.44	0.40	0.37	0.50	0.43	0.39	0.36	0.46	0.39	0.35	0.31	0.34	0.31	0.28	0.25	0.18	0.17	0.18	0.19	0.14
	60°	0.48	0.43	0.40	0.36	0.47	0.42	0.39	0.35	0.42	0.35	0.31	0.27	0.29	0.25	0.22	0.20	0.09	0.10	0.11	0.12	-
	50°	0.48	0.45	0.42	0.39	0.47	0.44	0.41	0.38	0.40	0.36	0.32	0.29	0.23	0.21	0.17	0.15	-	-	-	-	-
	40°	0.52	0.48	0.45	0.43	0.51	0.47	0.44	0.42	0.41	0.38	0.35	0.34	-	-	-	-	-	-	-	-	-
	30°	0.62	0.58	0.54	0.52	0.61	0.57	0.53	0.51	-	-	-	-	-	-	-	-	-	-	-	-	-
	20°	0.81	0.76	0.70	0.67	-	-	-	-	-	-	-	-	-	-	-	-	-	-	-	-	-
Dip direction of the closer spaced joint set is against the direction of flow	20°	0.62	0.55	0.68	0.77	-	-	-	-	-	-	-	-	-	-	-	-	-	-	-	-	-
	30°	0.51	0.60	0.66	0.70	0.61	0.56	0.70	0.79	-	-	-	-	-	-	-	-	-	-	-	-	-
	40°	0.48	0.55	0.59	0.61	0.50	0.59	0.65	0.69	0.54	0.57	0.70	0.79	-	-	-	-	-	-	-	-	-
	50°	0.48	0.53	0.56	0.58	0.47	0.53	0.57	0.60	0.46	0.56	0.62	0.66	0.42	0.55	0.68	0.77	-	-	-	-	-
	60°	0.52	0.58	0.61	0.63	0.47	0.51	0.54	0.57	0.42	0.47	0.51	0.54	0.34	0.47	0.53	0.56	0.27	0.27	0.62	0.69	-
	70°	0.62	0.73	0.78	0.82	0.51	0.58	0.62	0.65	0.40	0.44	0.48	0.50	0.29	0.33	0.36	0.38	0.18	0.18	0.30	0.32	0.23
	80°	0.81	1.14	1.20	1.26	0.61	0.94	0.98	1.02	0.41	0.74	0.76	0.78	0.23	0.49	0.51	0.53	0.09	0.24	0.28	0.32	0.14
	85°	1.23	1.28	1.33	1.38	1.08	1.13	1.18	1.23	0.97	0.99	1.01	1.03	0.66	0.70	0.74	0.78	0.46	0.51	0.56	0.61	0.42

1: Apparent dip angle of the closer spaced joint set in a vertical plane containing direction of flow

4.3. *Steps for determining the value of Js for non-orthogonal fractured systems*

Assuming that a geological formation is mainly fractured by two joint sets, data collected from the field can be interpreted by stereographic projection to determine the mean planes of dip and dip direction of each joint set. The *Js* value can then be determined as follows:

- Draw the two planes representing the two joint sets;
- Draw the vector representing the direction of flow;
- Determine the α angle between the two planes of joint sets along the flow direction vector;
- Determine the closer spaced joint set according to the joint spacing of both joint sets;
- Determine the apparent dip of the closer spaced joint sets along the flow direction vector;
- Determine the dip direction of the closer spaced joint set relative to the direction of flow (in or against the direction of flow);
- Determine the RJS of the two joint sets.

Since the α angle, the apparent dip of the closer spaced joint set, the dip direction of the closer spaced joint set relative to the direction of flow and the RJS are determined, Table 3 (if $\alpha > 90°$) and Table 4 (if $\alpha < 90°$) can be used to determine the *Js* value.

5. Impact of α angle

The root mean square error (RMSE) is used as a standard statistical measure of model performance in meteorology, air quality, climate research studies, etc. In the field of geosciences, the RMSE is often used to assess modeling quality both in terms of accuracy and precision (Gokceoglu and Zorlu, 2004; Jones et al., 2003; Wise, 2000; Zimmerman et al., 1999). As shown in Eq. (18), the RMSE parameter corresponds to the mean of the differences between the *Js* obtained by considering the modification associated to α and the standard *Js*

proposed by Kirsten for an orthogonal system. For this study, the RMSE value indicates the importance of the error produced when the used *Js* does not correspond to that of the studied case. A higher RMSE value indicates a considerable difference between our proposed values of *Js* and the standard values proposed by Kirsten.

$$RMSE = \left(\frac{1}{n}\sum_{i=1}^{n}\left(Js_{orthogonal} - Js_{\propto angle}\right)^2\right)^{1/2} \quad (18)$$

The produced RMSE results are shown in Fig. 18. The RMSE value (expressed in %) for a given α angle is the average value of RMSE determined according to all considered angles of the closer spaced joints set. According to Fig. 18, the RMSE is proportional to the difference between the α angle and the 90° angle used by Kirsten. The RMSE values when α < 90° are greater than those when α > 90°. Given the obtained RMSE, assuming a non-orthogonal fractured system rather than an orthogonal fractured system can produce considerable error when determining the erodibility index.

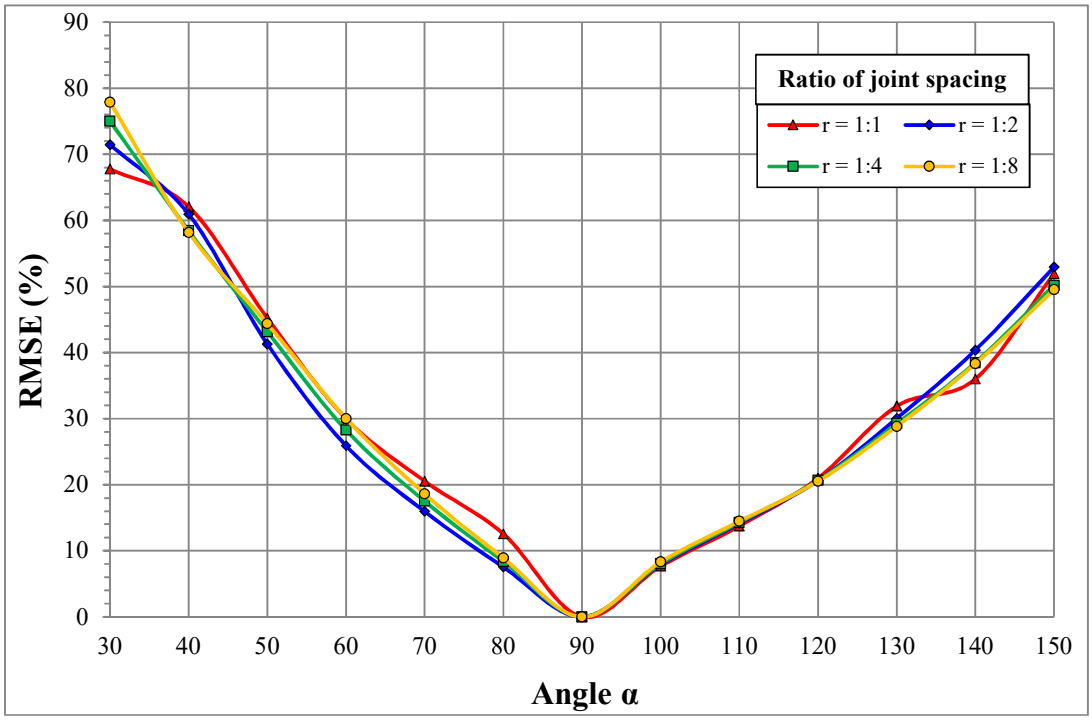

Fig. 18. Graphical representation of RMSE versus α.

To illustrate these findings, three cases examined by Pells (2016) and originally studied by Van Schalkwyk et al. (1994), are analyzed with the *Js* values proposed in this study for a non-orthogonal fractured system. The three case studies are from the spillways of dams located in South Africa: the rock mass section 8E-1 of the Mokolo Dam, the rock mass section 9E-2 of the Hartebeespoort Dam and the rock mass section 13E-3 of the Marico-Bosved Dam. The data for the examined sections, as related to Kirsten's index factors, include the compressive strength of intact rock (*Ms*), the rock block size (*Kb*), the discontinuity shear strength (*Kd*) and the relative block structure (*Js*); the data are presented in Table 5. The *Js* values adopted by Van Schalkwyk et al. (1994) assumed an orthogonal fractured system ($\alpha = 90°$). From the adopted *Js* value of each examined section, the RJS, the dip direction of the closer spaced joint set relative to the direction of flow and the dip of the closer spaced joint set are determined using Table 2 (Kirsten, 1982). This information is then used to calculate the corresponding *Js* when $\alpha > 90°$ (from 100° to 150°) by considering the proposed *Js* rating as presented in Table 3. The corresponding *Js* values are presented in Table 5. Subsequently, Kirsten's index is calculated according to the corresponding *Js* values (Table 6).

The values obtained for Kirsten's index for the three examined sections, calculated as a function of α, are converted into required hydraulic stream power (P_r) using Eq. (19) as proposed by Annandale (1995, 2006). Note that all examined case studies of Annandale (1995, 2006) are considered to be orthogonal fractured systems. The determined required hydraulic stream power for the three examined sections are presented in Table 6 and shown in Fig. 19.

$$P_r = N^{0.75} \tag{19}$$

Table 5. Data for the analyzed case studies.

						α angle					
						100°	110°	120°	130°	140°	150°
Case study	*Ms*	*Kb*	*Kd*	*Js* (90°)	r[1]-Direction[2]-Dip[3]	*Js*					
8E-1	140	25.45	0.94	0.81	2-against-5°	0.72	0.6	0.48	0.31	0.27	0.18
9E-2	70	16.47	1.00	1.20	2-in-5°	1.13	1.02	0.96	0.90	0.79	0.65
13E-3	140	26.95	1.68	0.69	4-against-10°	0.64	0.50	0.36	0.22	0.11	0.05

The information below are determined using data from Table 2 of Kirsten (1982) based on the Js *value*
1: Ratio of joint spacing
2: Dip direction of closer spaced joint set relative to the direction of flow, either in or against direction of flow
3: Dip angle of the closer spaced joint set

Table 6. Calculations of the required hydraulic stream power.

Case study	8E-1		9E-2		13E-3	
α angle	*N*	P_r	*N*	P_r	*N*	P_r
90°	2713	376	1380	226	4752	572
100°	2411	344	1303	217	4056	508
110°	2009	300	1176	201	3169	422
120°	1608	254	1107	192	2282	330
130°	1038	183	1037	183	1394	228
140°	904	165	911	166	697	136
150°	603	122	749	143	317	75

N: Kirsten's index
P_r: Required hydraulic steam power

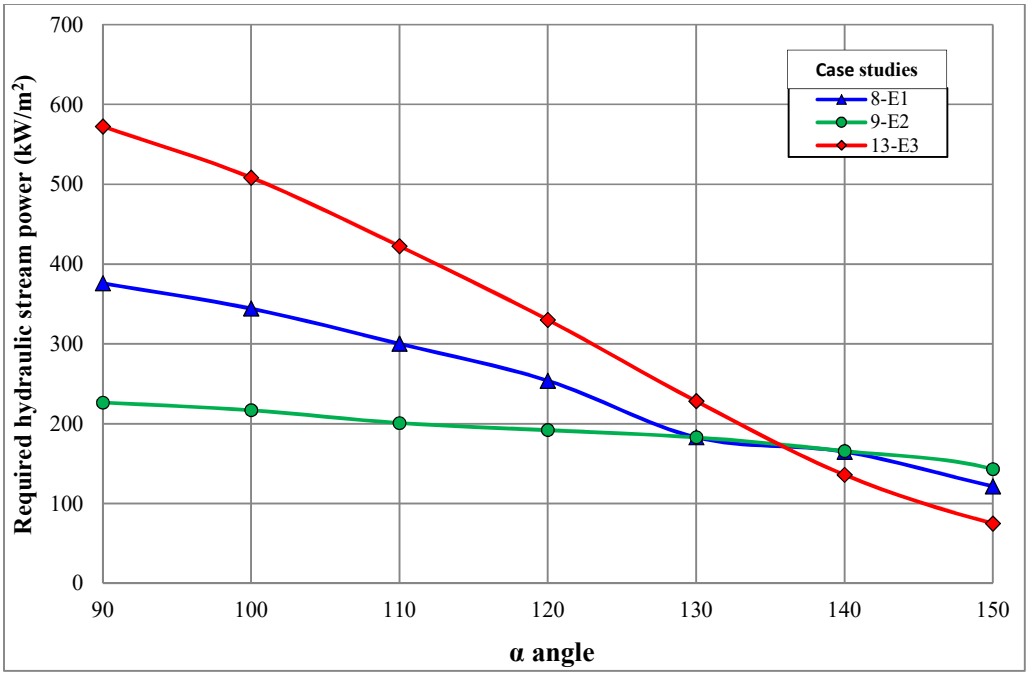

Fig. 19. Graphical representation of the required hydraulic stream power versus α.

According to Fig. 19, the required hydraulic stream power for the three examined sections has an inversely proportional relationship to α. Thus, when α > 90°, there is a decreasing trend of the required hydraulic stream power. Indeed, the greatest difference in terms of the required hydraulic stream power occurs between the standard angle of 90° and the α of 150°. This confirms the previously established findings regarding RMSE, where the largest error (when α > 90°) is observed at α = 150°. Moreover, the required hydraulic stream power, using α = 150° for the 13-E3, 8-E1 and 9-E2 case studies, is reduced by an order of 7, 3 and 1.5 times, respectively, when compared to the required hydraulic stream power when α = 90° (see Fig. 19 and Table 6). Although the 13E-3 rock mass has the highest factor values for *Ms*, *Kb* and *Kd* (Table 5), there is a marked decreasing curve of the required hydraulic stream power. This is explained by the effect of *Js*. Indeed, the lowest *Js* values, according to α, are noted for rock mass 13E-3 (Table 5). These findings highlight the importance of considering α when determining Kirsten's index to calculate the required hydraulic stream power.

6. Conclusion

Adjustments are introduced to Kirsten's initial concept concerning the relative block structure parameter. Thus, equations are proposed to determine the relative block structure parameter when the fractured system is non-orthogonal, where the angle between the planes of the two joint sets is larger or smaller than the 90° angle considered by Kirsten. Two equations are proposed; the first assesses the relative block structure when the blocks are oriented in the direction of flow, while the second is used when blocks are oriented against the direction of flow. The use of the two proposed equations, by varying the angle between the two joint sets (α angle), makes it possible to propose a rating for the relative block structure parameter when α is larger or smaller than the standard angle of 90°.

According to our analyses, assuming an orthogonal fractured system in cases represented by a non-orthogonal fractured system can create discrepancies in the determination of the erodibility index and, consequently, in the assessment of the hydraulic erodibility of rock. The non-orthogonal fractured systems reflect cases that can be found in the field where rock's vulnerability to erosion will differ if one assumes an orthogonal fractured system. Accordingly, our proposed rating of *Js* for non-orthogonal fractured systems can provide a more accurate assessment of the hydraulic erodibility of rock.

Conflict of interest

The authors wish to confirm that there are no known conflicts of interest associated with this publication and there has been no significant financial support for this work that could have influenced its outcome.

Acknowledgement

The authors would like to thank the organizations that have funded this project: Natural Sciences and Engineering Research Council of Canada (Grant No 498020-16), Hydro-Quebec (NC-525700) and Mitacs Accelerate program (Grant Ref. IT10008). The authors would acknowledge the useful assistance of Dr Hendrik Kirsten and Professor Monte Van Schalkwayk.

References

Annandale GW. Scour Technology, Mechanics and Engineering in Practice. McGraw-Hill, New York; 2006.

Annandale GW. Erodibility. Journal of Hydraulic Research 1995;33:471–94.

Annandale GW, Kirsten HAD. On the erodibility of rock and other earth materials. Hydraulic

Engineering 1994;1:68–72.
Basarir H, Karpuz C. A rippability classification system for marls in lignite mines. Engineering Geology 2004;74:303–18.
Bieniawski ZT. Engineering rock mass classifications : a complete manual for engineers and geologists in mining, civil, and petroleum engineering 1989:251.
Bollaert E, Munodawafa MC, Mazvidza DZ. Kariba Dam Plunge Pool Scour : quasi-3D Numerical Predictions. Proceeding of 6th International Conference on Scour and Erosion, Paris, 2012, p. 627–34.
Castillo LG, Carrillo JM. Scour, velocities and pressures evaluations produced by spillway and outlets of dam. Water 2016;8:1–21.
Clark PB. Rock mass and rippability evaluation for a proposed open pit mine at Globe-Progress, near Reefton. Master of Science in Engineering Geology, University of Canterbury, New Zealand; 1996.
Doog N. Die hidrouliese erodeerbaarheid van rotmassas in onbelynde oorlope met spesiale verwysing na die rol van naatvulmateriaal. Master thesis in Afrikaans language, University of Pretoria, South Africa (cited in Pells, 2016).; 1993.
Gokceoglu C, Zorlu K. A fuzzy model to predict the uniaxial compressive strength and the modulus of elasticity of a problematic rock. Engineering Applications of Artificial Intelligence 2004;17:61–72.
Hahn WF, Drain MA. Investigation of the erosion potential of kingsley dam emergency spillway. Proceeding of the joint Annual Meeting and Conference of AIPG, AGWT, and the Florida Section of AIPG, Orlando, Florida, USA., 2010, p. 1–10.
Huang MW, Liao JJ, Pan YW, Cheng MH. Modifications of the erodibility index method for the evaluation of the soft bedrock erosion. 47th US Rock Mechanics / Geomechanics Symposium, 2013, p. 7.
Jones NL, Davis RJ, Sabbah W. A comparison of three-dimensional interpolation techniques for plume characterization. Ground Water 2003;41:411–9.
Keaton JR. Estimating erodible rock durability and geotechnical parameters for scour analysis. Environmental & Engineering Geoscience 2013;4:319–43.
Kirkaldie L. Rock classification systems for engineering purposes. American Society for Testing and Materials, ASTM STP-984, Philadephia, PA 1988.
Kirsten HAD. Case histories of groundmass characterization for excavatability. Rock Classification Systems for Enginering Purposes American Society for Testing and Materials, STP 984 1988:102–20.
Kirsten HAD. A classification system for excavation in natural materials. The Civil Engineer in South Africa 1982;24:292–308.
Kirsten HAD, Moore JS, Kirsten LH, Temple DM. Erodibility criterion for auxiliary spillways of dams. Journal of Sediment Research 2000;15:93–107.
Laugier F, Leturcq T, Blancer B. Stabilité des barrages en crue : Méthodes d'estimation du risque d'érodabilité aval des fondations soumises à déversement par-dessus la crête. Proceeding de la Fondation des barrages. Chambery, France, 2015, p. 125–36.
Lowe J, Chao PC, Luecker AR. Tarbela service spillway plunge pool development. Water Power Dam Construction 1979;31:85–90.
MacGregor F, Fell R, Mostyn GR, Hocking G, McNally G. The estimation of rock rippability. Quarterly Journal of Engineering Geology 1994;27:123–44.
Moore JS, Kirsten HAD. Discussion – Critique of the rock material classification procedure. Rock classification systems for engineering purposes. American Society for Testing and Materials, STP-984, L. Kirkaldie Ed, Philadephia, 1988, p. 55–8.
Moore JS, Temple DM, Kirsten HAD. Headcut advance threshold in earth spillways. Bulletin of the Association of Engineering Geologists 1994;31:277–80.

Mörén L, Sjöberg J. Rock erosion in spillway channels – A case study of the Ligga spillway. Proceedings of 11th Congress of the International Society for Rock Mechanics, Lisbon, Portugal, 2007, p. 87–90.
Pells SE. Erosion of rock in spillways. Ph.D Thesis, University of New South Wales, Australia; 2016.
Pells SE, Pells PJN, Peirson WL, Douglas K, Fell R. Erosion of unlined spillways In Rock - does a "scour threshold" exist? Proceeding of Australian National Committee on Large Dams . Brisbane, Queensland, Australie, 2015, p. 1–9.
Pitsiou S. The effect of discontinuites of the erodibility of rock in unlined spillways of dams. Master's Thesis, University of Pretoria, South Africa; 1990.
Rock AJ. A semi-empirical assessment of plung pool scour: Two-dimensional application of Annandale's Erodibility Method on four dams in British Colombia, Canada. Master's Thesis, University of British Columbia. Vancouver, British Columbia, Canada; 2015.
Van Schalkwyk A, Jordaan J, Dooge N. Erosion of rock in unlined spillways. Proceeding of International Commission on Large Dams, Paris, 71 (37), 1994, p. 555–71.
United States Department of Agriculture (USDA). Field procedures guide for the headcut erodibility index, Chapter 52, Part 628 Dams. vol. 628. 1997.
Wise S. Assessing the quality for hydrological applications of digital elevation models derived from contours. Hydrological Processes 2000;14:1909–29.
Wyllie C, Mah W. Rock slope engineering civil and mining. In: Hoek, E. and Bray, J.W., Eds., Rock slope Engineering, Taylor & Francis Group, London and New York; 2004.
Zimmerman D, Pavlik C, Ruggles A, Armstrong MP. An experimental comparison of ordinary and universal kriging and inverse distance weighting. Mathematical Geology 1999;31:375–90.